

SPRINGER
REFERENCE

Ambarish Goswami
Prahlad Vadakkepat
Editors

Humanoid Robotics: A Reference

on tendon-driven systems is introduced. The tendon-driven hands with N -type tendon system with intrinsic actuation and underactuated hand with extrinsic actuation are presented as the case studies.

1 Introduction

A hand is an end effector device with multiple fingers attached to a palm. It is a very complicated mechanical device that plays key role in manipulation. Human daily tasks involve tasks as holding objects, holding bars for assisting body balance, and applying impacts to objects using tools. The design of a hand requires dexterity, robustness, and high-output force, even for performing daily human tasks.

In human hands, there are two types of actuation: intrinsic muscle and extrinsic muscle. Intrinsic muscles reside in the palm, which are connected to finger joints with tendons. Extrinsic muscles are located in the forearm, which are connected to finger joints with tendons that go through the wrist. In human hand, large portion of the actuation is done with extrinsic muscle. Some muscles of the thumbs and some small muscles are intrinsic.

It is rather straightforward to design robot hands with tendon-driven systems. Already in early sixteenth century, Leonardo Da Vinci made a drawing of dissected human hand, which clearly shows the tendon-driven structure of a human hand.

Tendon-driven hands are built using intrinsic actuators, extrinsic actuators, or the combination of them. Tendon-driven hands with extrinsic muscle have a benefit that the large actuator can be used to actuate finger joints. Only small actuators would fit in phalanxes of fingers. To design a hand with large force capacity, the hand would become oversized if actuators must fit in phalanxes. It also implies the benefit of using large reducers. The gearboxes that fit in finger joints would be miniature, which leads to fragile hand. On the other hand, extrinsic muscles have complex routing of tendons through the wrist. For the hand that needs to be modular from the rest of the robot, the use of intrinsic actuators is desirable.

The finger mechanism developed by Yamashita [21] is one of the earliest studies of mechanical hand. This hand is not explicitly anthropomorphic, but the effort to generate sufficient fingertip force to perform grasping tasks results in placing pneumatic actuators in the base of the hand, which are connected to finger joints with tendons.

Utah/MIT hand [6, 7] and Stanford/JPL hand [17, 18] are pioneers of modern tendon-driven robot hands. Utah/MIT hand uses steel belts as tendons and leads them to pneumatic actuators placed in forearm with idler pulleys. Stanford/JPL hand uses wire ropes as tendons that are connected to pulleys connected to motors. Bowden cables, or bicycle brake cables, are used to route tendons.

More recently, Shadow hand [16], DLR hand-arm system [3, 4], Pisa [1], iCub hand [19], and robot hands developed in The University of Tokyo [8, 20] are examples of tendon-driven hands.

In this chapter, basic theory and issues of tendon-driven systems are introduced. Tendon structure, underactuation, tendon routing, and tension sensing are treated. Two design examples of the tendon-driven hands with N -type tendon system and underactuated hand are presented.

2 Basic Structure of Tendon-Driven Systems

Wire-driven systems are categorized into three types as shown in Fig. 1 according to the number of actuators used in the system. The N -type tendon-driven system uses N actuators to drive N DOF (degree of freedom). Tendon topology inherently forms a closed loop due to the unilateral constraint of tendon tension. When tension of f is applied to a tendon, tension of a tendon increases by f on one side, whereas it decreases by f on the other side. Since tension on a tendon can never be negative, a tendon will become slack when the tension becomes zero. Slack tendon will incur nonlinear behavior and should be avoided in many cases. To avoid the tendons from getting slack, bias or initial tension f_0 should be applied to the tendons. Under the bias, tension becomes $f + f_0$ on one side and $f_0 - f$ on the other side. The value of the bias should be chosen to satisfy $f_0 \geq \max f$ to avoid the tendon getting slack under any operating conditions.

Slack wires introduce nonlinear behavior to the system, and it is a cause of wire's derailing from the pulleys. The N -type wire system requires minimum number of actuators, but proper pretensioning mechanisms are necessary for each tendon loop.

The tendon f and the joint torque τ have the following static relationship:

$$\tau = J^T f \quad (1)$$

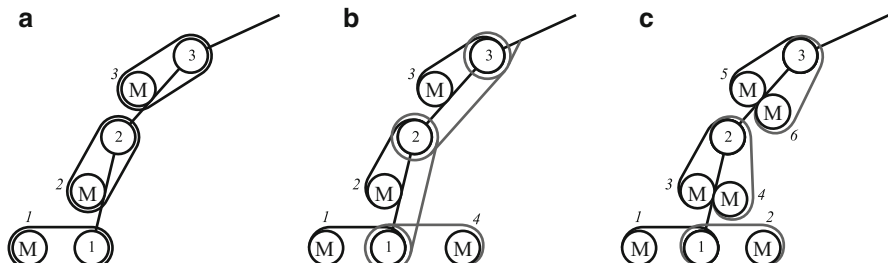


Fig. 1 Commonly used tendon systems used in robot hands. $1, 2, 3, \dots$ are joint numbers and $1, 2, 3, \dots$ are actuator numbers. (a) N type tendon system. (b) $N+1$ type tendon system. (c) $2N$ type tendon system

Here, J is the Jacobian matrix of the tendon displacement \mathbf{x} and the joint angle \mathbf{q} .

$$J = \frac{\partial \mathbf{x}}{\partial \mathbf{q}} \quad (2)$$

The tension required for realizing the joint torque can be formulated as the problem of finding the inverse relation of (1).

In the case of Fig. 1a, the joint torque τ and the actuator torque τ_a have the following relation with unit reduction ratio.

$$\tau = \begin{bmatrix} 1 & 0 & 0 \\ 0 & 1 & 0 \\ 0 & 0 & 1 \end{bmatrix} \tau_a \quad (3)$$

If the J is non-singular, there is one-to-one relationship between τ and τ_a , which can be found with the following equation:

$$\tau_a = (J^T)^{-1} \tau \quad (4)$$

In order to have control over the tension, $2N$ -type wire actuation can be used. In $2N$ systems, both end of the tendons are attached to different actuators. Link being driven is attached to the middle of the tendon. The link is actuated by the difference of the tendon tension. This way, arbitrary tension can be applied to the tendon regardless of the actuation torque, to maintain tendons from getting slack. Utah/MIT hand [6] is one of the examples of the hand with $2N$ -type tendon system.

In the case of Fig. 1a, the joint torque τ and the tendon tension f have the following relation with unit pulley radius:

$$\tau = \begin{bmatrix} 1 & -1 & 0 & 0 & 0 & 0 \\ 0 & 0 & 1 & -1 & 0 & 0 \\ 0 & 0 & 0 & 0 & 1 & -1 \end{bmatrix} f \quad (5)$$

Here, the J is column full rank, and we can find the inverse relation as follows:

$$f = (J^T)^\# \tau + \left(I - (J^T)^\# J^T \right) \xi \quad (6)$$

The operator $\#$ shows the Moore-Penrose pseudo-inverse. The first term shows the least square solution, and the second term shows null space mapping of the tension. We can choose arbitrary vector ξ to realize desirable tension while realizing τ .

In the example of (5),

$$\mathbf{f} = \begin{bmatrix} 1/2 & 0 & 0 \\ -1/2 & 0 & 0 \\ 0 & 1/2 & 0 \\ 0 & -1/2 & 0 \\ 0 & 0 & 1/2 \\ 0 & 0 & -1/2 \end{bmatrix} \boldsymbol{\tau} + \begin{bmatrix} 1/2 & 1/2 & 0 & 0 & 0 & 0 \\ 1/2 & 1/2 & 0 & 0 & 0 & 0 \\ 0 & 0 & 1/2 & 1/2 & 0 & 0 \\ 0 & 0 & 1/2 & 1/2 & 0 & 0 \\ 0 & 0 & 0 & 0 & 1/2 & 1/2 \\ 0 & 0 & 0 & 0 & 1/2 & 1/2 \end{bmatrix} \boldsymbol{\xi} \quad (7)$$

gives the inverse relation. From this equation, it is clear that $\mathbf{f} > 0$ can be realized with choice of $\boldsymbol{\xi}$.

The minimum way to maintain the tension is the use of $N+1$ -type wire actuation. It was first used in tendon-driven manipulator by Morecki [13] and then adopted in robot hand by Stanford/JPL hand [18].

Let $J \in \mathbf{R}^{(n+1) \times n}$ be a Jacobian matrix that relates tendon displacement \mathbf{x} and joint angles \mathbf{q} . The wire tension that realizes the joint torque can be calculated by (6). Null space mapping of J^T has maximum rank of 1 for $N+1$ -type systems.

From this equation, with proper choice of $\boldsymbol{\xi}$, $\mathbf{f} > 0$ can be achieved when the null space has rank 1. The challenge in mechanical design is to route the tendons so the rank of the null space of J^T does not become 0.

For the example of Fig. 1b, the relation between the tendon tension and the joint torque is calculated as follows:

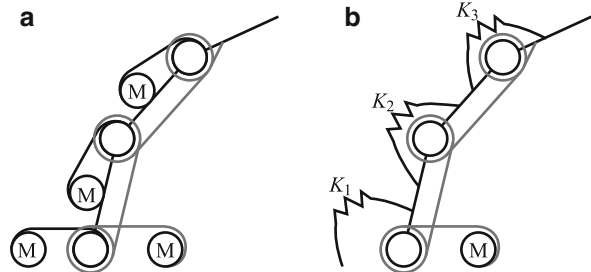
$$\boldsymbol{\tau} = \begin{bmatrix} 1 & 0 & 0 & -1 \\ 0 & 1 & 0 & -1 \\ 0 & 0 & 1 & -1 \end{bmatrix} \mathbf{f} \quad (8)$$

The following equation holds for the inverse relation. Proper choice of $\boldsymbol{\xi}$ enables $\mathbf{f} > 0$.

$$\mathbf{f} = \frac{1}{4} \begin{bmatrix} 3 & -1 & -1 \\ -1 & 3 & -1 \\ -1 & -1 & 3 \\ -1 & -1 & -1 \end{bmatrix} \boldsymbol{\tau} + \begin{bmatrix} 1 & 1 & 1 & 1 \\ 1 & 1 & 1 & 1 \\ 1 & 1 & 1 & 1 \\ 1 & 1 & 1 & 1 \end{bmatrix} \boldsymbol{\xi} \quad (9)$$

Another class of the tendon-driven system is the underactuated systems. In underactuated systems, number of DOF is larger than number of actuators. Figure 2 shows example of a fully actuated $N+1$ -type tendon system and a 3DOF 1 actuator underactuated tendon system. Underactuated hand shows mechanical adaptation to the grasped object, which enables stable power grasping without sophisticated control. In such systems, equilibrium is determined upon existence of the external force including return springs, even when the tendon is position controlled.

Fig. 2 Mechanism of fully actuated and underactuated tendon systems. (a) Fully actuated tendon system (N+1 Type). (b) Underactuated tendon system



The equation of motion of a finger can be written as follows:

$$M(\mathbf{q})\ddot{\mathbf{q}} + C(\mathbf{q}, \dot{\mathbf{q}})\dot{\mathbf{q}} - \frac{\partial V(\mathbf{q})}{\partial \mathbf{q}} = \boldsymbol{\tau} + \sum_{i=1}^{n_c} J_{c,i}^T \mathbf{f}_{ext,i} = J^T \boldsymbol{\tau} + J_c^T \mathbf{f}_{ext} \quad (10)$$

Here, M is the mass matrix and C is the sum of Coriolis term and damping term. Underactuated hand often is equipped with springs to determine coupling effect between joints due to the torque distribution effect. Spring effect that includes these springs is included in V as the elasticity potential. $J_{c,i}$ is a Jacobian matrix for i -th contact point, and $\mathbf{f}_{ext,i}$ is the wrench if i -th contact point. Also, $J_c = [J_{c,1}^T \cdots J_{c,n_c}^T]^T$ and $\mathbf{f}_{ext} = [\mathbf{f}_{ext,1}^T \cdots \mathbf{f}_{ext,n_c}^T]^T$.

The finger in Fig. 2b has actuation matrix and elastic potential function as follows:

$$\boldsymbol{\tau} = [-1 \ -1 \ -1]^T \boldsymbol{\tau} \quad (11)$$

$$V(\mathbf{q}) = \frac{1}{2} K_1 q_1^2 + \frac{1}{2} K_2 q_2^2 + \frac{1}{2} K_3 q_3^2 \quad (12)$$

When the finger is in a holonomic constraint, the equation of motion becomes the following form:

$$M(\mathbf{q})\ddot{\mathbf{q}} + C(\mathbf{q}, \dot{\mathbf{q}})\dot{\mathbf{q}} - \frac{\partial V(\mathbf{q})}{\partial \mathbf{q}} = \sum_{k=1}^{n_h} \lambda_k \frac{\partial \psi_k}{\partial \mathbf{q}} \quad (13)$$

where $\boldsymbol{\Psi} = [\psi_1 \cdots \psi_{n_h}]^T = \mathbf{0} \in \mathbf{R}^{n_h}$ are holonomic constraints that include constraint on tendon lengths and contact positions. n_h is the number of constraints and λ_k are Lagrangian multipliers.

In a static state, the constraint force and posture of the hand can be solved by solving the following equations:

$$\frac{\partial V(\mathbf{q})}{\partial \mathbf{q}} + \sum_{k=1}^{n_h} \lambda_k \frac{\partial \psi_k}{\partial \mathbf{q}} = \mathbf{0} \quad (14)$$

3 Tendon Routing

In tendon-driven systems, it is common to put actuators on base; thus tendons go through multiple joints. Depending on the routing of the tendons, tendons may either affect torque of multiple joints or decoupled from specific joints. Similar discussion was carried out for manipulator by Hirose and Ma [5]. One of the common way is to wrap the tendons around the pulleys at each joint as in Fig. 3a. In this case, tendons contribute to torque at the each joint. In the case of Fig. 3a, the actuation matrix is given as follows with unit radius of the pulleys:

$$\tau = \begin{bmatrix} 1 & 1 & 1 & -1 \\ 0 & 1 & 1 & -1 \\ 0 & 0 & 1 & -1 \end{bmatrix} f \quad (15)$$

It is beneficial that the joint near to the base that requires the largest torque will have contributions from all tendons. On the other hand, torque control requires control of all tendons. Also, tendons that are routed to distal joints require large range of motion, which will result in either slow movement or small tension.

This can be avoided by routing tendons through the center of proximal joint axes as shown in Fig. 3 (b1). In this tendon system, next relation holds for $i < j$, with x_i and q_j being tendon and joint displacement, respectively.

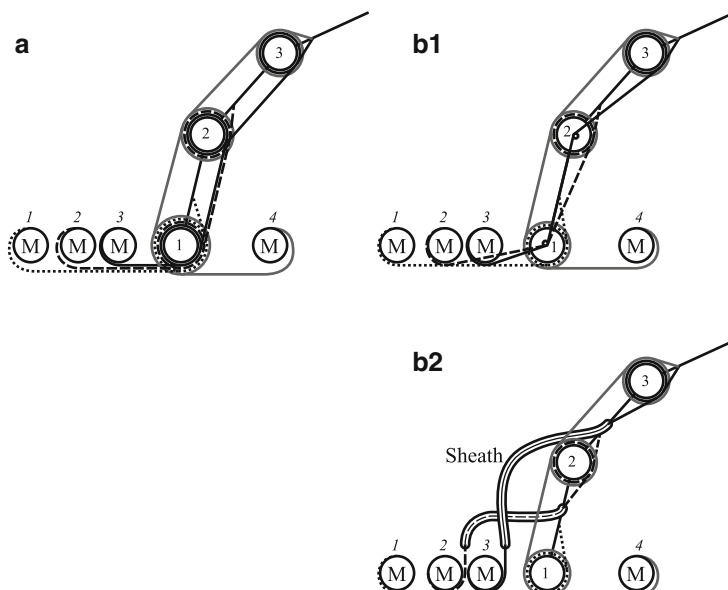


Fig. 3 Tendon systems with torque coupling and decoupling. 1, 2, 3, ... are joint numbers and 1, 2, 3, ... are actuator numbers. (a) Coupled tendon system with actuators on base (N+1 Type). (b1) Decoupled tendon system with routing pulleys (N+1 Type). (b2) Decoupled tendon system with sheaths (N+1 Type)

$$\frac{\partial x_i}{\partial q_j} = 0 \quad (16)$$

From virtual work principle, torque contribution of tendon i on joint j becomes zero, which means torque being decoupled. In the case of Fig. 3 (b1), the actuation matrix is given as follows with unit radius of the pulleys:

$$\tau = \begin{bmatrix} 1 & 0 & 0 & -1 \\ 0 & 1 & 0 & -1 \\ 0 & 0 & 1 & -1 \end{bmatrix} f \quad (17)$$

The same effect can be obtained by using sheaths as in Fig. 3 (b2). Bowden cables (or break wires) can be used in such configuration. The benefit of using sheaths is that they eliminate the necessity of the complicated pulley routing mechanism. Hence the hand can be made compact. However, sheaths have large and load-dependent nonlinear friction, which degrades force control performance.

In the examples above, circular pulley placed concentric to the joint axis was assumed as shown in Fig. 4a. With this structure, the moment arm is a constant value of the pulley radius r . The structure shown in Fig. 4b is also common. With this structure, moment arm varies with the joint angle θ . Let α be the angle between the finger link and the guide pulley as shown in Fig. 4b; the moment arm can be calculated as follows with r_0 being the moment arm at $\theta = 0$:

$$r(\theta) = \frac{\sin(\alpha + \frac{\theta}{2})}{\sin \alpha} r_0 \quad (18)$$

In this system, the moment arm changes from r_0 to $\frac{r_0}{\sin \alpha}$ as the joint angle moves from 0 to $\pi - 2\alpha$. This kind of tendon routing is beneficial in a case such as having a return spring at the joint. Since the return spring generates larger counter torque against the actuated torque as the joint angle increases, the fingertip force is lost at the large joint angle. This mechanism provides larger actuation torque at larger joint angle with same tendon tension, which has compensating effect to the return

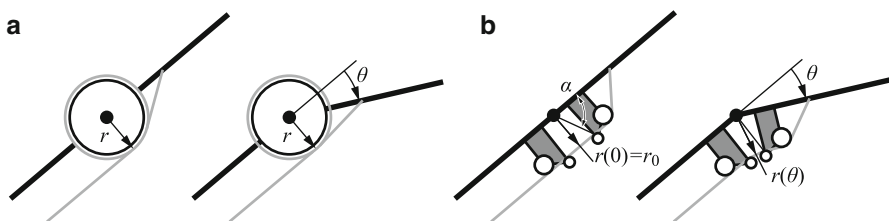


Fig. 4 Effect of joint structure to moment arm of tendon. (a) Case on concentric pulley. (b) Case on guide pulley

spring force. In the system with varying moment arm, the actuation matrix becomes a function of the joint angle. This mechanism is difficult to be used in N -type wire system that requires a tendon to form a loop with constant length. Consider a symmetric joint with guide pulleys on both the flexion and extension side. In this case, when the joint is flexed by θ , displacement of flexor tendon x_f is given as follows:

$$x_f = \int_{q=0}^{\theta} r(q) dq = -\frac{2 \cos(\alpha + \frac{\theta}{2})}{\sin \alpha} r_0 \quad (19)$$

Similarly, displacement of extensor tendon x_e is $x_e = \frac{2 \cos(\alpha - \frac{\theta}{2})}{\sin \alpha} r_0$; hence $x_f + x_e \neq 0$.

To route the tendons along the required path, adequate placement of the pulleys is necessary. Sheaths are used to route the tendons to avoid complexity. However, for the cases that the minimization of the tendon friction is desirable, the tendon should be routed using pulleys instead.

The arbitrary position and direction of a tendon can be realized with a pair of pulleys as shown in Fig. 5. If a tendon at initial configuration (input) intersects with final configuration (output), then only one pulley is necessary as shown in Fig. 5a. In this case, pulley axis n_i can be calculated as follows:

$$\mathbf{n}_i = \mathbf{a}_{in} \times \mathbf{a}_{out} \quad (20)$$

The center position of the pulley c_i can be found as an equidistance point from input and output tendon with distance of pulley radius r_i . For the case that the input tendon and output tendon do not intersect as in Fig. 5b, we can always find a line segment that intersects to with both the input and output tendon. The parameters of the line segment \mathbf{a}_{mid} and \mathbf{b}_{mid} are uniquely determined from intersection points on input tendon and output tendon, thus s_1 and s_2 . Since each deflection can be made

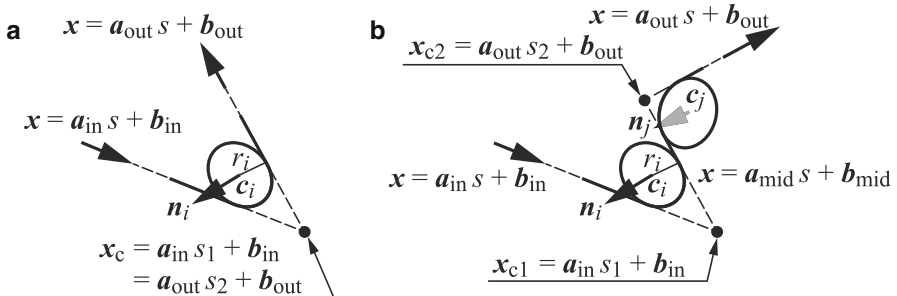


Fig. 5 Arbitrary tendon routing with pulleys. (a) Input line and output line having an intersecting point. (b) Input line and output line not having an intersecting point

with a pulley, which means only a pair of pulleys is necessary at maximum in either case, pulley position and orientation can be calculated for each deflection as in the previous case.

4 Tension Sensing of Tendon Driven Systems

Tension sensing is an important technology in force-controlled tendon-driven systems. The simplest method to measure the tension of the tendon is by a load cell directly inserted serially in the tendon (as shown in Fig. 6). This way, the tension T can directly be measured by the load cell. However, this method adds the moving weight to the tendon that would result in low resonant frequency thus loss of mobility performance. The alternative way to measure the tension is to measure the reaction force of the motor pulley as in Fig. 6 (b1). This way, the load cell can be fixed to stationary base. Torque measurement of the pulley axis as in Fig. 6 (b2) can also be used. Strain gauge-based force transducer is the most commonly used technique to measure the force or torque. For hydraulic actuators, pressure measurement can also be used. Force transducer can be any type without loss of generality.

To measure a tension acting on a tendon, mechanism as in Fig. 6c is often used. Salisbury and Craig [18] used similar mechanism to measure the tension on Stanford/JPL hand. The tendon angle θ can be chosen so that the maximum tension and measurement range of the load cell will coincide. For this mechanism to measure the tension correctly, either the high stiffness force transducer or pulley displacement measurement is necessary.

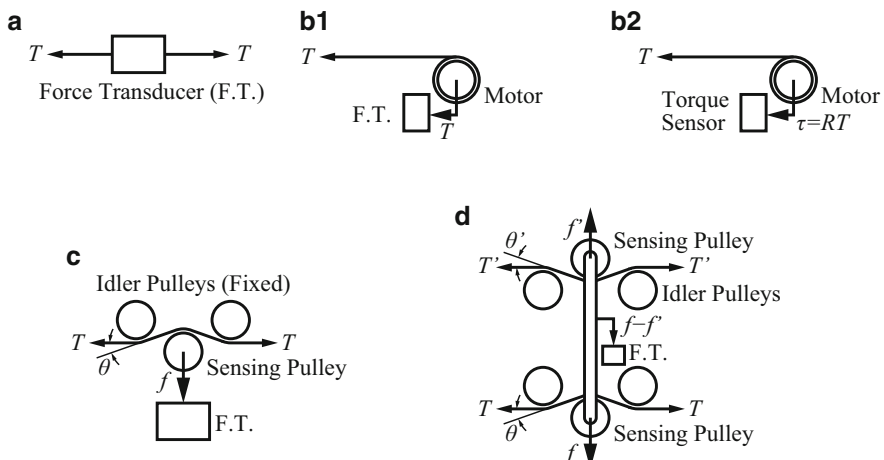


Fig. 6 Measurement mechanism of tendon tension. (a) Series measurement. (b1) Source measurement (Reaction Force). (b2) Source measurement (Reaction Torque). (c) Pulley measurement. (d) Differential pulley measurement

In tendon-driven systems, the difference of the tendon tension is converted to the joint torque. From this perspective, differential measurement of the tendon tension is desirable in many cases. Figure 6d is the differential measurement method proposed by Kaneko et al. [10].

5 Example: N-Type Tendon-Driven Hand with Intrinsic Actuators

One of the challenges in robot hand design is the robustness of the actuators and transmissions that tend to be very small. The robot hand using electro-hydrostatic actuators [9] is one of the attempt to realize robustness and force sensitivity by using backdrivable hydraulic actuators. In this hand, hydraulic actuator called electro-hydrostatic actuators (EHAs) is used to realize backdrivability, robustness, and force controllability. See Fig. 7 for structure of a revolute EHA. Hydraulic vane motors were installed in the finger joints, and pump and electric motor were installed in forearm.

There were two hydraulic tubes connecting each pump and vane motor. These tubes must be flexible to enable fingers from flexing and extending without burden. However, flexible tubes have low-pressure tolerance, which lead to the use of low hydraulic fluid pressure that implies larger hydraulic components for the same torque output.

To design hydraulic systems with higher operating pressure, hydraulic portion of the actuation system must be built as a solid block. In such systems, motion of the actuator needs to be transmitted to joints of the fingers. The concept of [8] is to design a hand with hydraulic actuator cluster and passive tendon-driven hand mechanism that can be detached easily.

See Fig. 7 for structure of a revolute EHA used in the *N*-type tendon-driven hand.

Auxiliary circuits were added to the EHA used in [9]. Vacuum check valves prevent cavitation by supplying hydraulic oil to the system when the pressure drops below specified value. Relief valves protect the system from overpressure when a large external force was applied (Fig. 8).

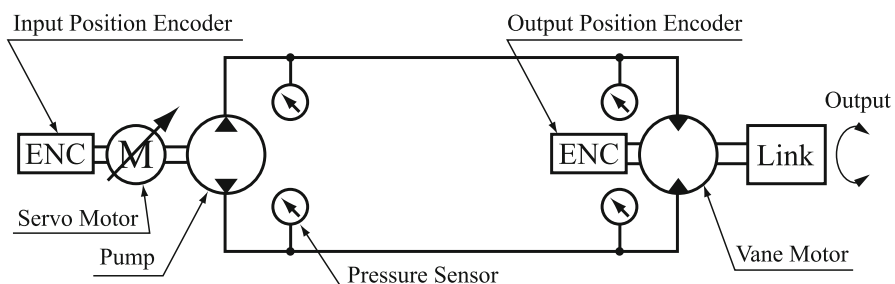


Fig. 7 Basic structure of a revolute electro-hydrostatic actuator

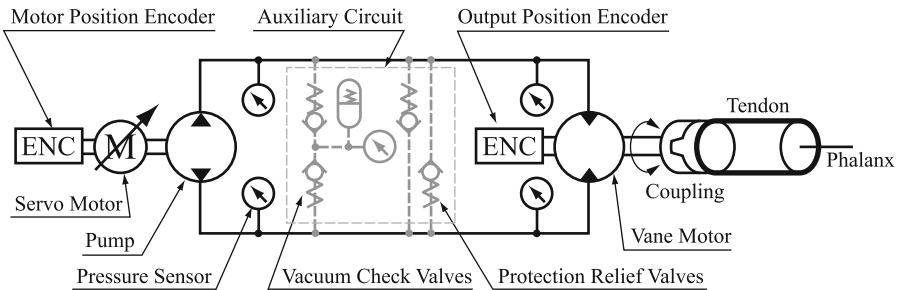


Fig. 8 Structure of a revolute electro-hydrostatic actuator used in *N*-type tendon-driven hand

Fig. 9 Structure of an *N*-type tendon-driven hand with intrinsic revolute electro-hydrostatic actuator

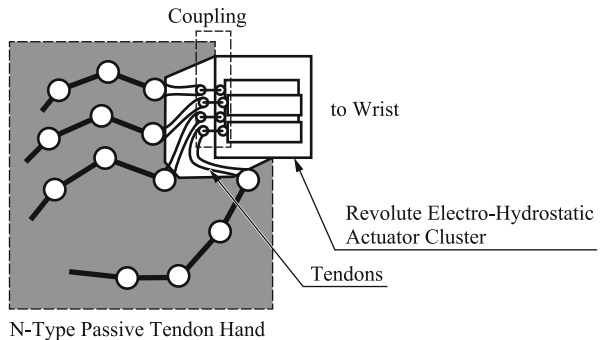
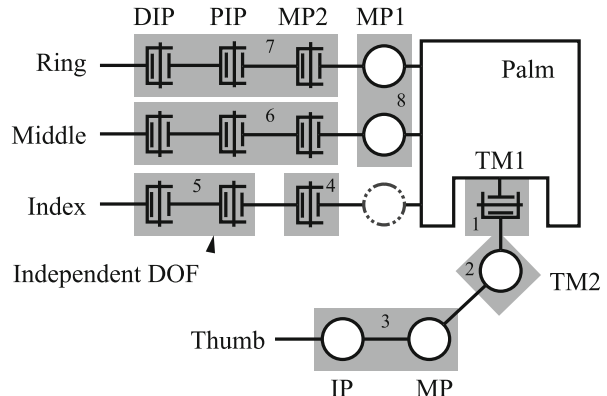


Fig. 10 Joint and DOF placement of the *N*-type tendon-driven hand



The passive wire hand was designed using *N*-type tendon system. Actuators are placed in palm, which are attached to the pulleys that are connected to tendons. The connection between pulleys and actuators is done through coupling. The structure of the actuation system is shown in Fig. 9.

8 DOF were selected as shown in Fig. 10 based on grasp shape analysis with Cutkosky's grasp taxonomy [2]. The thumb was placed opposing the index finger. The designed hand was capable of performing 12 out of 15 grasp patterns [8].

Force acting on fingers is measured indirectly by hydraulic pressure. In hydraulic systems, the following relationship holds between actuator torque (or force) and actuator displacement:

$$\tau = \frac{\partial V_1}{\partial q} p_1 - \frac{\partial V_2}{\partial q} p_2 \quad (21)$$

Here, p_1 and p_2 are pressure acting on chambers, V_1 and V_2 are volumetric displacement of the corresponding chamber, τ is the output torque, and q is the actuator displacement.

For the symmetric hydraulic motors or cylinders, this relation is simplified as follows with p being the differential pressure:

$$\tau = \frac{\partial V}{\partial q} p \quad (22)$$

$\frac{\partial V}{\partial q}$ is the generalized form of piston area in case of cylinders. In N -type tendon-driven hand, pulley tension was estimated from pressure measurement of hydraulic vane motors.

All fingers were designed to be modular and identical. Fingers have the tendon routing as shown in Fig. 11. In all fingers, two distal joints are rigidly coupled; thus the hand is fully actuated. The thumb uses all 3 DOF. The index finger uses 2 DOF for flexion and extension. MP1 joint of the index finger is locked and not used. For middle and ring finger, tendons that drive DIP and PIP joints (τ_3) are locked. In the design shown in Fig. 11, fingers with less DOF will produce proper motion just by locking unnecessary tendons. The tendon routing structure implies the actuation matrix being lower triangular. The all tendons are routed using pulleys and bearings to minimize friction and gain maximum backdrivability.

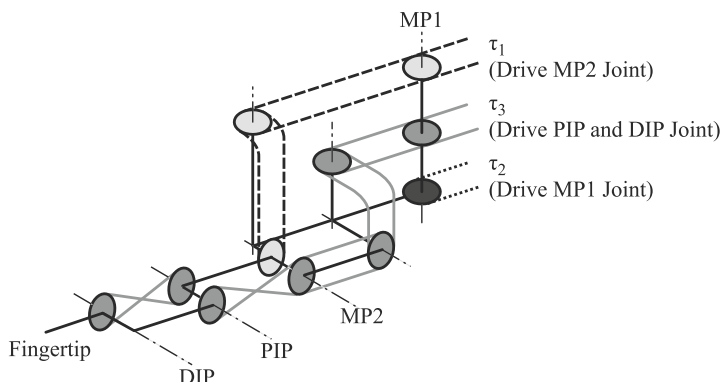


Fig. 11 Tendon routing of N -type 3DOF finger with 4 joints

Fig. 12 Tendon routing in palm structure that aligns pulleys on a surface

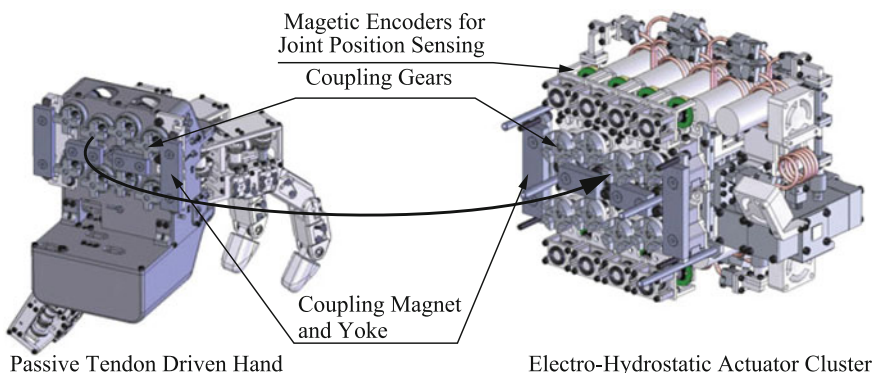
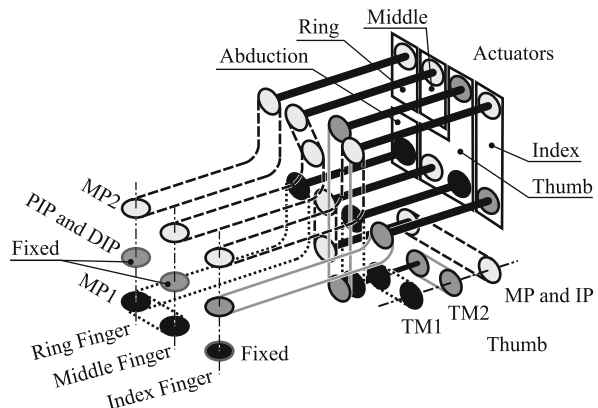


Fig. 13 Coupling design of the tendon-driven hand and the actuator cluster

Since the hand is fully actuated and the movement is deterministic, position measurement is done with encoders attached to the vane motors. Magnetic absolute encoders are used.

All tendons from the fingers are terminated at the pulleys with axes facing to the actuator cluster. Figure 12 shows the tendon routing in the palm that aligns pulleys on the coupling surface.

Figure 13 shows the design of the coupling between passive tendon-driven hand and the EHA cluster. Coupling between the actuator cluster and the pulleys is done with cross-shaped wedge. The coupling wedges on the wire hand side are axially spring loaded so that the compression force will act between the couplings on the actuator and the hand. Permanent magnets are used to hold the hand and the actuator cluster together.

The outlook of the hand is shown in Fig. 14. The hand was capable of being impedance controlled utilizing the backdrivability of the hand and the electro-hydrostatic actuators as reported in [8]. Tension measurement was done by torque measurement at the actuator using hydraulic pressure measurement.

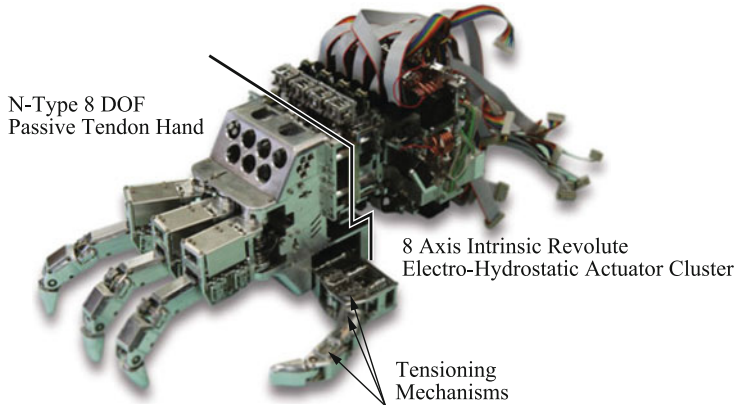


Fig. 14 Outlook of the *N*-type tendon-driven hand

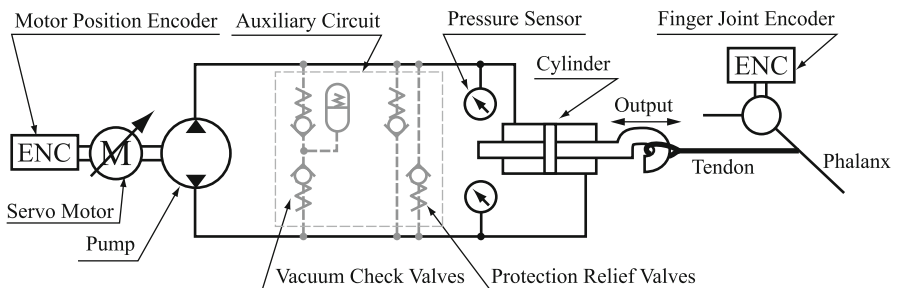


Fig. 15 Structure of a prismatic electro-hydrostatic actuator for tendon-driven hand

6 Example: Robot Hand with Underactuated Tendon Drives

One of the challenges in design of a robot hand that is used as an end effector of the robots is the size and weight reduction. Underactuated hand is a useful technique in such systems because of the small number of the actuators and the mechanical adaptation to the grasped object without control.

Robustness is another issue of a hand design. A hand is the first upper limb link to get in contact with environment. It must be sufficiently dexterous; at the same time, it must be endured from unexpected collision.

Force controllability and backdrivability are important qualities in designing a light weight, robust, and dexterous hand. Treratanakulwong et al. [20] proposed a low-friction underactuated tendon-driven hand for extrinsic linear electro-hydrostatic actuators shown in Figs. 15 and 16. Low-friction tendon system ensures force controllability of electro-hydrostatic actuators. Tension measurement is done with pressure sensors at cylinders. Kang et al. [11] reported a linear electro-hydrostatic actuator cluster, which is connected to the hand.

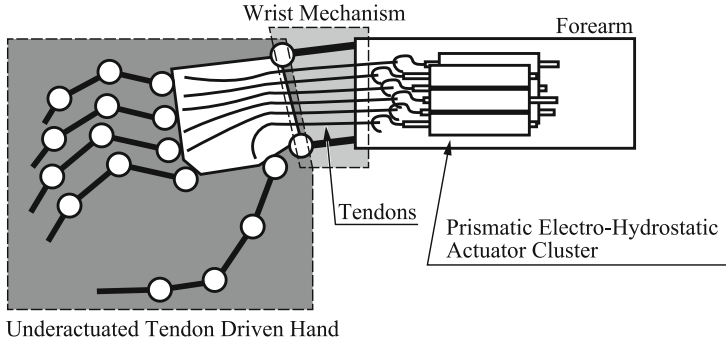


Fig. 16 Structure of an underactuated tendon-driven hand with extrinsic prismatic electro-hydrostatic actuator

In general, it is difficult to perform precision grasping with underactuated hands. Underactuated hand needs fine-tuning of the return springs for the hand to perform deterministic movement under absence of the load, which is important in performing precision grasping. Ozawa et al. [14, 15] proposed an elastic coupling mechanism. In this mechanism, underactuated joints are connected with springs to perform fully actuated movement when there is no force being applied to the finger. When the finger gets in contact with an object, the finger will start to show underactuated behavior when more tension is applied to the tendon.

Consider a case with an underactuated finger with only extension springs. Putting $V(\mathbf{q})$ as a potential function of springs, stiffness matrix $K = \frac{\partial V(\mathbf{q})}{\partial \mathbf{q}}$ will be diagonal. Adding coupling springs is identical to adding off-diagonal components to the stiffness matrix. We can explicitly set the stiffness of the coupling with this method.

Based on this idea, Treratanakulwong et al. [20] developed an underactuated hand with 5 fingers, 20 joints, and 12 tendons as shown in Fig. 17. The design of [14] was extended for the finger with less actuators and extension springs. The index and middle finger are equipped with 2 active DOF flexion. DIP and PIP joints are coupled with spring. The ring and little finger have 1 active DOF. The abduction joints were driven in underactuated manner. The thumb was placed opposing to the middle finger. Since the thumb has three-dimensional joint axis placement, $N + 1$ -type tendon system is used. All the finger joints are equipped with magnetic encoders.

The tendon configuration of the 2 DOF fingers and 1 DOF fingers are shown in Figs. 18 and 19, respectively. The stack of the pulley layers is installed in the 3D-printed finger phalanges. The $N + 1$ tendon configuration of the thumb is shown in Fig. 20. For the MP2, joint of index and middle fingers requires large torque. In these fingers, guide pulleys were used in the MP2 joint to increase the moment arm at large flex angle.

For the underactuated hands, finger posture is not determined with actuator position. Magnetic absolute encoders are installed at each of the joint to know the posture. Actuator position is calculated from the finger posture. Encoders with SPI

Fig. 17 Joint and DOF placement of the underactuated tendon-driven hand

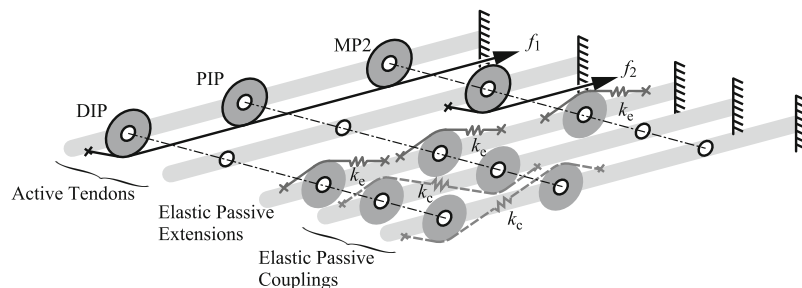
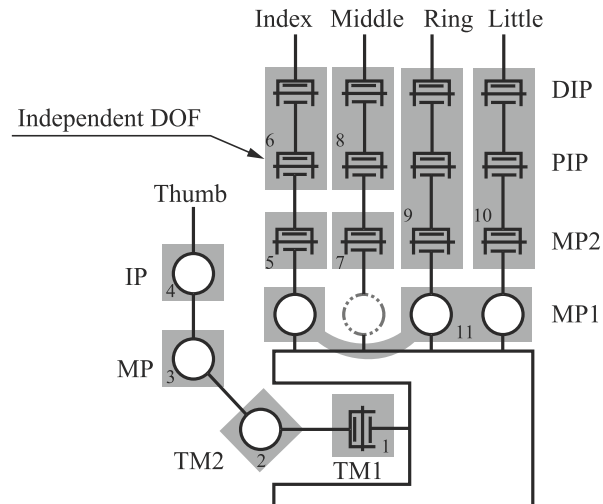


Fig. 18 Tendon routing and spring structure of 2DOF fingers

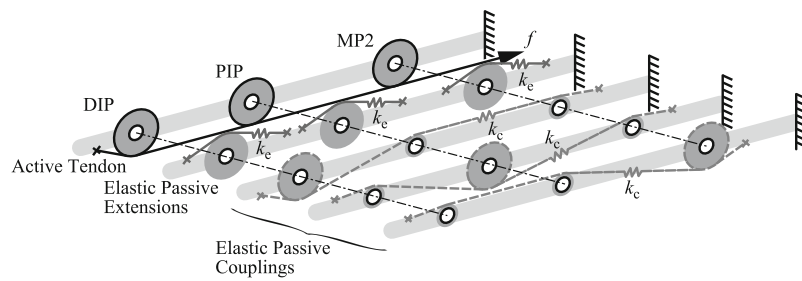


Fig. 19 Tendon routing and spring structure of 1DOF fingers

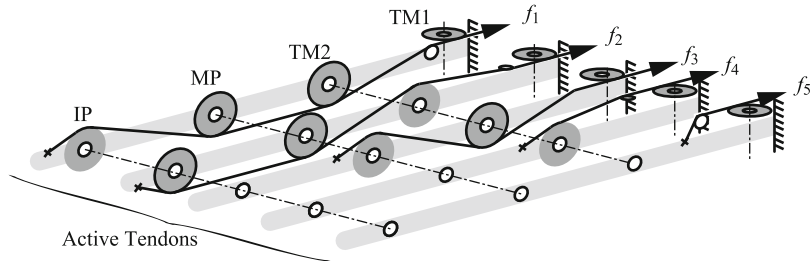


Fig. 20 N+1-type tendon routing structure of the thumb

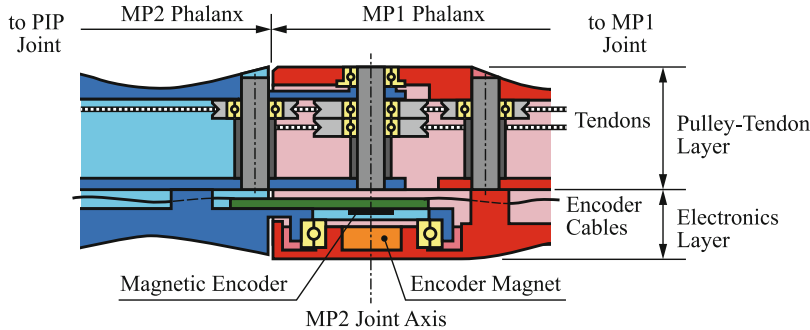


Fig. 21 Cross section of finger structure

(serial peripheral interface) and with daisy chain capability are used to minimize the encoder cabling.

Figure 21 shows the cross section of a finger. The finger consists of two layers: pulley-tendon layer and electronics layer. The layered structure protects cabling of magnetic encoders.

One of the challenges of designing a tendon-driven hand with extrinsic actuators on the forearm is to design tendon routing through the wrist. In a human hand, carpal bones and a flexor retinaculum form a fibro-osseous tunnel to route tendons coming from fingers to extrinsic muscles through the wrist [12]. Sheaths prevent tendons from abrasion.

Sheaths have been used in many cases [16, 18] to simplify tendon routing mechanism. However, even for low friction materials such as PTFE, which has friction coefficient of 0.05, the friction coefficient is about the double of that of the ball bearings.

Treratanakulwong et al. [20] proposed a formulation of a tendon routing problem as an optimization problem. The pulley configuration \mathbf{n}_i and \mathbf{c}_i can be parametrized with the line parameter s_i and the angle θ_i that the tendon wraps around a pulley, when r_i are given.

The proposed optimization is as follows with $\mathbf{s} = [s_1 \dots s_n]^T$ and $\boldsymbol{\theta} = [\theta_1 \dots \theta_n]^T$:

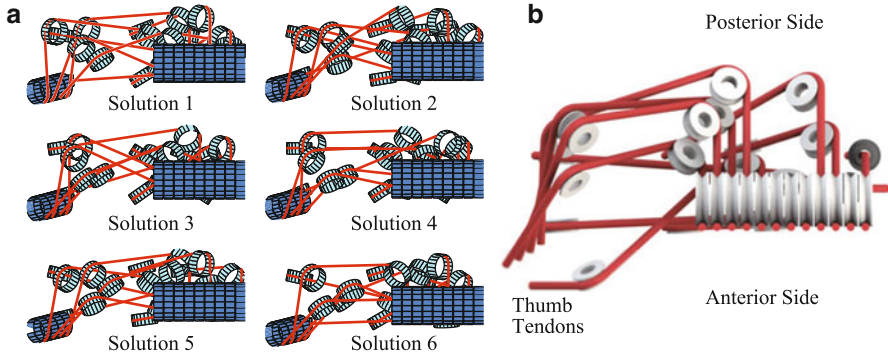


Fig. 22 Pulley configuration optimization result and actual design (*right hand*). **(a)** Some of the possible solutions from different initial conditions. **(b)** Final pulley configuration after manual modifications from solution 1

$$\{s^*, \theta^*\} = \underset{\{s, \theta\}}{\operatorname{argmin}} \sum_{i \neq j} \left\{ \frac{1}{\|c_i - c_j\|} + \alpha (||c_i - c_j|| - r_t) \right\} \quad (23)$$

subject to:

$$s_{\min} \leq s \leq s_{\max} \quad (24)$$

$$\theta_{\min} \leq \theta \leq \theta_{\max} \quad (25)$$

The first term prevents the pulleys from colliding each other. The second term is the penalty to the pulleys becoming too far apart. α is the weight and r_t is the minimum bounding sphere of the pulleys. Sequential quadratic programming engine of MATLAB was used for the optimization. Since the optimization is highly nonlinear, the local minimum solution is dependent on the initial condition. Figure 22 shows the local minima from different initial conditions and the final configuration after tuning by manual modifications that enable assembly.

The outlook of the hand is shown in Fig. 23a, b. The wires are aligned so that it can be connected to 14 axes of miniature linear cluster electro-hydrostatic actuator [11].

Figure 23c shows the implementation of the tendon aligning pulleys designed with the proposed optimization. With conventional material removal fabrication process, realization of this mechanism would be difficult and costly. Additive fabrication process using 3D printing was used to overcome this issue. Similar fabrication is possible using laser sintering metal 3D printers.

Figure 24 shows power grasping with the underactuated hand. Figure 24b shows the posture when the hand is closed without an object. Figure 24c shows the posture with a cylindrical object in the hand. The hand was operated with identical tendon tension, but the hand adapted to the object due to the underactuated structure.

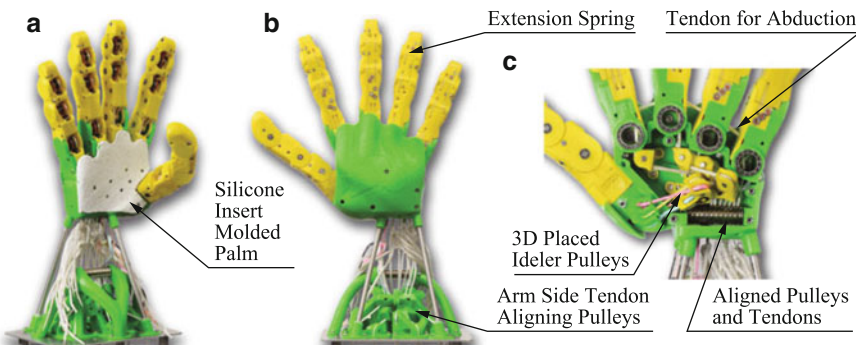
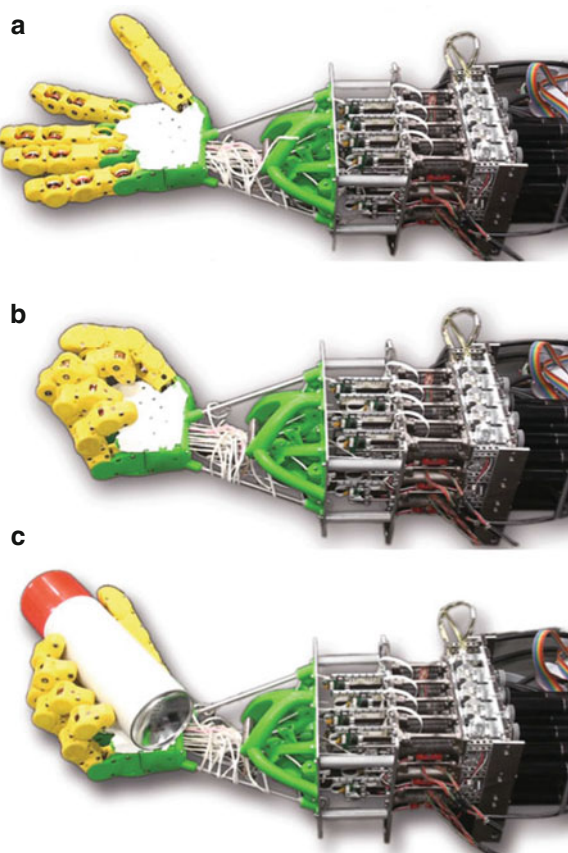


Fig. 23 Outlook of the underactuated hand. (a) Palm view (Anterior Side). (b) Backside view (Posterior Side). (c) Tendon aligning pulley structure (Posterior Side)

Fig. 24 Power grasping with underactuated hand. (a) Open hand. (b) Closing hand. (c) Power grasping cylindrical object



7 Future Directions and Open Problems

In this chapter, the basic theory of the tendon-driven systems, tendon routing, and tendon tension sensing is treated. Also, an N -type tendon-driven hand with intrinsic actuators and an underactuated hand with extrinsic actuators were shown as the examples of the implementation. N -type tendon-driven hand realized modularized compact implementation of a hand, and the elastic coupling realized fully actuated hand at low grasping force and underactuated hand at high grasping force without an additional actuator.

Additive manufacturing technology has enabled hollow monocoque exoskeletal link structures that hold pulleys inside, which is beneficial in protecting fragile tendon systems from collisions. Extensive use of 3D printing will occur for tendon-driven systems.

The use of synergies together with underactuated hand is another trend. Both of the technologies will not only contribute in reducing the mechanical resources but also reducing the necessity of complicated control by utilizing physical properties.

One of the open problems is the optimization between complexity and low friction. Although the pulley system reduces the friction, it increases the mechanical complexity. Complex mechanical system increases the size and weight and deteriorates reliability. The use of combination of the pulleys and the sheaths should be considered, but design methodology is yet to be investigated. For the hand to gain higher dexterity, larger number of actuator is necessary. However, tendon-driven systems with higher complexity may require different ways of control. Analytic method based on computing Jacobian matrix may become difficult.

The design of a palm is a mechanical open issue. The flexibility of the palm plays an important role in the human hand. However, in robot hand, especially for the hand with pulley routing, tendon routing will become very difficult if there are additional joints in metacarpal bones.

One of the practical open problems is the automatic tendon routing. Although the routing became partially automatic, it still requires much hand tuning due to the following problems. First, surfaces that the axes of bearings fit should be machined with removal process due to the precision and surface roughness of the 3D printers. Hence these holes should be accessible by mill machines. Next, there are many cases that the optimization fails. Setting a via point of a tendon route may solve such failure, but there is no systematic way of setting such points. Another practical issue is the tendon termination. Termination is one of the weakest points of a tendon.

References

1. M.G. Catalano, G. Grioli, E. Farnioli, A. Serio, C. Piazzaand, A. Bicchi, Adaptive synergies for the design and control of the Pisa/IIT softhand. *Int. J. Robot. Res.* **33**(5), 768–782 (2014). <https://doi.org/10.1177/0278364913518998>
2. M.R. Cutkosky, Grasp choice, grasp models, and the design of hands for manufacturing tasks. *IEEE Trans. Robot. Autom.* **5**(3), 269–279 (1989). <https://doi.org/10.1109/70.34763>

3. M. Grebenstein, A. Albu-Schäffer, T. Bahls, M. Chalon, O. Eiberger, W. Friedl, R. Gruber, S. Haddadin, U. Hagn, R. Haslinger, H. Höppner, S. Jörg, M. Nickl, A. Nothelfer, F. Petit, J. Reill, N. Seitz, T. Wimböck, S. Wolf, T. Wüsthoff, G. Hirzinger, The DLR hand arm system, in *Proceedings of International Conference on Robotics and Automation*, 2011, pp. 3175–3182. <https://doi.org/10.1109/ICRA.2011.5980371>
4. M. Grebenstein, M. Chalon, W. Friedl, S. Haddadin, T. Wimböck, G. Hirzinger, R. Siegwart, The hand of the DLR hand arm system: designed for interaction. *Int J Robot. Res.* **31**(13), 1531–1555 (2012). <https://doi.org/10.1177/0278364912459209>
5. S. Hirose, S. Ma, Coupled tendon-driven multijoint manipulator, in *Proceedings of IEEE International Conference on Robotics and Automation*, 1991, pp. 1268–1275. <https://doi.org/10.1109/ROBOT.1991.131786>
6. S.C. Jacobsen, E.K. Iversen, D.F. Knutti, R.T. Johnson, K.B. Biggers, Design of the Utah/M.I.T. dexterous hand, in *Proceedings of IEEE International Conference on Robotics and Automation*, vol. 3, 1986, pp. 1520–1532. <https://doi.org/10.1109/ROBOT.1986.1087395>
7. S.C. Jacobsen, J.E. Wood, D.F. Knutti, K.B. Biggers, E.K. Iversen, The Utah/MIT dexterous hand: work in progress, in *Proceedings of International Symposium of Robotics Research*, 1984, pp. 601–653.
8. H. Kaminaga, J. Ono, Y. Shimoyama, T. Amari, Y. Katayama, Y. Nakamura, Anthropomorphic robot hand with hydrostatic cluster actuator and detachable passive wire mechanism, in *Proceedings of IEEE International Conference on Humanoid Robots*, 2009, pp. 1–6. <https://doi.org/10.1109/ICHR.2009.5379528>
9. H. Kaminaga, T. Yamamoto, J. Ono, Y. Nakamura, Backdrivable miniature hydrostatic transmission for actuation of anthropomorphic robot hands, in *Proceedings of IEEE International Conference on Humanoid Robots*, 2007, pp. 36–41. <https://doi.org/10.1109/ICHR.2007.4813846>
10. M. Kaneko, K. Yokoi, K. Tanie, On a new torque sensor for tendon drive fingers. *IEEE Trans. Robot. Autom.* **6**(4), 501–507 (1990). <https://doi.org/10.1109/70.59362>
11. T. Kang, H. Kaminaga, Y. Nakamura, A robot hand driven by hydraulic cluster actuators, in *Proceedings of IEEE International Conference on Humanoid Robots*, 2014, pp. 39–44. <https://doi.org/10.1109/HUMANOIDS.2014.7041335>
12. I.A. Kapandji, *The Physiology of the Joints*, vol. 1, 5th edn., Upper Limb. (Churchill Livingstone, 1982)
13. A. Morecki, Synthesis and control of the anthropomorphic two-handed manipulator, in *Proceedings of 10th International Symposium on Industrial Robots*, 1980, pp. 461–474.
14. R. Ozawa, K. Hashirii, H. Kobayashi, Design and control of underactuated tendon-driven mechanisms, in *Proceedings of IEEE International Conference on Robotics and Automation*, 2009, pp. 1522–1527. <https://doi.org/10.1109/ROBOT.2009.5152222>
15. R. Ozawa, H. Kobayashi, K. Hashirii, Analysis, classification, and design of tendon-driven mechanisms. *IEEE Trans. Robot.* **30**(2), 396–410 (2014). <https://doi.org/10.1109/TRO.2013.2287976>
16. F. Röthling, R. Haschke, J.J. Steil, H. Ritter, Platform portable anthropomorphic grasping with the Bielefeld 20-DOF Shadow and 9-DOF TUM hand, in *Proceedings of IEEE International Conference on Intelligent Robots and Systems*, 2007, pp. 2951–2956. <https://doi.org/10.1109/IROS.2007.4398963>
17. J.K. Salisbury, Design and control of an articulated hand, in *Proceedings of the 1st International Symposium on Design and Synthesis*, 1984
18. J.K. Salisbury, J.J. Craig, Articulated hands: force control and kinematic issues. *Int. J. Robot. Res.* **1**(1), 4–17 (1982). <https://doi.org/10.1177/027836498200100102>
19. A. Schmitz, U. Pattacini, F. Nori, L. Natale, G. Metta, G. Sandini, Design, realization and sensorization of the dexterous icub hand, in *Proceedings of IEEE International Conference on Humanoid Robots*, 2010, pp. 186–191. <https://doi.org/10.1109/ICHR.2010.5686825>
20. T. Treratanakulwong, H. Kaminaga, Y. Nakamura, Low-friction tendon-driven robot hand with carpal tunnel mechanism in the palm by optimal 3D allocation of pulleys, in *Proceedings*

- of IEEE International Conference on Robotics and Automation, 2014, pp. 6739–6744.
<https://doi.org/10.1109/ICRA.2014.6907854>
21. T. Yamashita, Mechanical fingers controlled by machine and their applications to materials handling. J. Soc. Instrum. Control. Eng. 3(6), 429–439 (1964).
<https://doi.org/10.11499/sicejl1962.3.429> (in Japanese)



DLR Multi-fingered Hands

Markus Grebenstein, Maxime Chalon, Máximo A. Roa,
and Christoph Borst

Contents

1	Introduction	482
2	DLR Hand I	484
2.1	Design	485
2.2	Results and Lessons Learned	488
3	DLR Hand II	489
3.1	Design	489
3.2	Results and Lessons Learned	494
4	Spacehand	496
4.1	Design	496
4.2	Results and Lessons Learned	500
5	Awipi Hand	500
5.1	Motivation and Goals	501
5.2	Design	502
5.3	Results and Lessons Learned	514
6	Final Discussion	517
	References	518

Abstract

This chapter describes the history of development of multi-fingered hands at the Institute of Robotics and Mechatronics, German Aerospace Center (DLR). It provides an overview of kinematics, actuators, and sensors used in different

M. Grebenstein (✉)

Department of Mechatronic Components and Systems, Institute of Robotics and Mechatronics,
German Aerospace Center (DLR), Wessling, Germany
e-mail: markus.grebenstein@dlr.de

M. Chalon · M. A. Roa · C. Borst

Institute of Robotics and Mechatronics, German Aerospace Center (DLR), Wessling, Germany
e-mail: maxime.chalon@dlr.de; maximo.roa@dlr.de; christoph.borst@dlr.de

hands, including *DLR Hand I* and *DLR Hand II*, *Spacehand* and *Awiwi Hand*, discussing also the lessons learned during the development process and the usage of the hands. A more in-depth description of the most recent DLR development, the *Awiwi Hand*, is provided to illustrate in detail the challenges of the design of robotic hands, including the consideration of functional aspects that guarantee achieving the required performance in these end effectors.

Acronyms

DIP	Distal interphalangeal joint.
DLR	German Aerospace Center.
DoF	Degree of freedom.
DSP	Digital signal processor.
FPGA	Field programmable gate array.
FSR	Force-sensitive resistor.
GEO	Geostationary earth orbit.
HMC	Hamatometacarpal joint.
IP	Interphalangeal joint.
JPL	Jet Propulsion Laboratory.
LEO	Lower earth orbit.
MC	Metacarpophalangeal joint.
MP	Metacarpophalangeal joint of the thumb.
PHRI	Physical human robot interaction.
PIP	Proximal interphalangeal joint.
PSD	(Optical) Position sensitive device.
PU	Polyurethane.
TCP	Tool center point.
TMC	Trapezometacarpal joint.

1 Introduction

The Institute of Robotics and Mechatronics at DLR is focused on the development of robotics for space applications. Hence, the driving factor of robotic hand development at DLR is the application of robots in dangerous and remote environments that are also unstructured, unknown, and unpredictable. To reach this ambitious goal there are two major research areas related to robotic hands, namely, design of dexterous robot hands and development of autonomous grasping capabilities. Naturally, the development of advanced autonomous grasping algorithms calls also

for very capable dexterous hands, driven by the requirements of the application itself as well as from the need for dexterous, robust, and easy to use platforms for software development.

The range of hands developed at DLR spans from a first three-fingered gripper (the first three-fingered gripper was called the “Melkschemel”, milking stool in English) in 1997 [8] to the highly anthropomorphic *Awiwi Hand* [29]. The following sections provide an overview of the DLR hand designs, their goals and requirements, as well as the achieved results and lessons learned during the development process, with a focus on the *Awiwi Hand* as the most performant, complex, and versatile hand built at DLR. Section 2 discusses *DLR Hand I*, the first hand designed with the intention of being an universal, dexterous multi-fingered hand that could be used in different robots, which required electronics and drives being fully integrated into the mechanical design. Section 3 illustrates *DLR Hand II*, an improved version of *DLR Hand I*, aiming at improved performance in terms of speed, grasping force, grasping performance, and reliability. Section 4 describes the *Spacehand*, a third redesign of the fully integrated hand concept of *DLR Hand I* intended for, and adapted to, space applications, using a new modularization concept. Finally, Sect. 5 highlights the anthropomorphic *Awiwi Hand* in two versions, designed for having human-like grasping performance, with the inherent robustness and dynamical behavior required to tackle the challenges of humanlike grasping in complex scenarios.

For the convenience of the reader, the acronyms and anatomical terms used in this chapter are provided above. Figure 1 provides a short introduction of the most important anatomical terms used in this chapter.

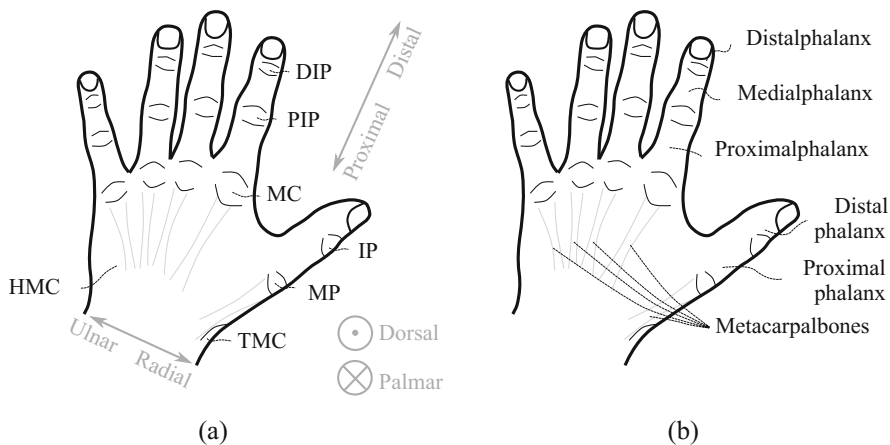


Fig. 1 Anatomical terminology used in the following chapters. Abbreviations: DIP distal interphalangeal, PIP proximal interphalangeal, MC metacarpophalangeal, IP interphalangeal, MP metacarpophalangeal, TMC trapezometacarpal, HMC hamatometacarpal. (a) Joints and positioning. (b) Bones

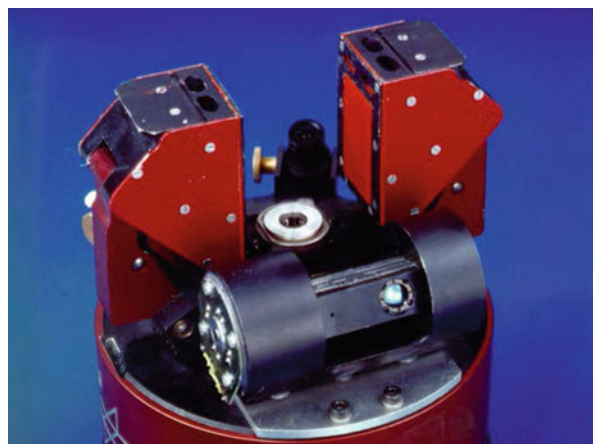
2 DLR Hand I

In 1993, during the Spacelab-D2 Mission, DLR performed a series of experiments onboard the Spacelab to verify the performance of a multi-axis robot in a space environment. These experiments, known as ROTEX [33, 34], impressively showed that most of the common tasks on space stations, such as handling drawers, doors, and bayonet closures, can be successfully performed with a two-fingered gripper as the *DLR ROTEX Gripper* (Fig. 2). In this particular case, the experimental environment was specifically designed for robot interaction. From these days, it was evident that future space missions would increasingly need *Space Robot Assistants* capable of performing a variety of tasks similar to the human, which created a strong demand for versatile and robust multi-fingered hands.

The design of multi-fingered hands has been an active area of research since the early 1970s. Initial robotic hands did not have all the actuators and electronics integrated into the palm [38, 50, 57], which is a must for a hand meant to fit any existing robot without major impact on its kinematics. In fact, a too large distance between the robot tool center point (TCP) and the center of the palm requires large elbow motions to change the hand orientation. Hence, it drastically reduces the workspace of the robot, in particular in obstacle-rich environments. The first hand developed to suit the needs of future robotics space missions, called *DLR Hand I* [8, 35], was designed considering these restrictions. To meet the requirements of a fully integrated hand applicable to arbitrary robots, the design goals were the following:

- Size close to the average human hand (a maximum size of 1.5 times the human hand was set as design requirement).
- Four fingers in the hand, to reduce the size and complexity of the final design (during fine manipulation at least three fingers must be in contact to securely hold the object, while a fourth finger is changing its contact location.)

Fig. 2 The *DLR ROTEX Gripper* used in the Spacelab-D2 Space Mission [34]. Experiments included autonomously catching a free-flying polyhedron in space using the two-finger gripper. This parallel jaw gripper was equipped with torque and proximity sensors, as well as a laser scanner. It is the origin of the so-called “artificial muscle” used in *DLR Hand I*



- Modular fingers to reduce the design complexity
- Full integration of the actuation into the hand body

2.1 Design

A short overview of the design of DLR Hand I is given below, focusing on kinematics design, actuation, and sensor equipment and concluding with the lessons learned while designing, operating, and using *DLR Hand I*.

2.1.1 Kinematics

The *DLR Hand I* (Fig. 3) is a four-fingered dexterous robot hand with a semi-anthropomorphic design. To reduce the complexity of the system, this modular hand consists of four identical fingers. Hence, the design space for the hand kinematics is pretty limited. Each finger comprises a two degree of freedom (DoF) cardanic base joint with intersecting axes for flexion/extension and for abduction/adduction, and two interphalangeal joints with one DoF. The two interphalangeal joints are coupled in a 1:1.05 ratio. The first axis of rotation of the base joint points toward inside the palm, and is perpendicular with respect to the middle plane, but tilted to the palm center with respect to the palmar surface of the base (Fig. 5c). To simplify the design, all subsequent axes were chosen as parallel. The length of the phalanges has been largely influenced by two constraints: the actuator must fit into the proximal phalanx, and the maximum finger length should be below 1.5 times the length of the human finger (the length of the average German male middle finger according to DIN 33402 is 84 mm, and the length at 95th percentile is 93 mm.) The link length and the ranges of motion of *DLR Hand I* and the human hand according to [7] are given in Table 1.

Fig. 3 *DLR Hand I* mounted on the *DLR Lightweight Robot I*. The hand can be used on an arbitrary robot due to the full integration of all drives and electronics inside the hand body. It is equipped with position and force sensors to enable compliance control. Tactile sensors attached to the finger surface provide contact point information, as well as the magnitude of the applied force



Table 1 Link lengths for the fingers of *DLR Hand I* vs. human middle finger, as reported in [7]

Phalanx	Overall	Proximal	Medial	Distal
Length <i>DLR Hand I</i>	173.35 mm	97.35 mm	40 mm	36 mm
Relative ratio	1	0.56	0.23	0.21
Length human hand	92.25 mm	44.6 mm	26.3 mm	17.4 mm +3.95 mm (tissue)
Relative ratio	1	0.48	0.29	0.23

Table 2 Finger range of motion (hardware limits) at each joint: MC joint (MC 1 and 2), PIP joint, and DIP joint

Finger	MC1	MC2	PIP	DIP ^a
Flexion	70°	–	100°	105°
Extension	20°	–	0°	0°
Abduction	–	30°	–	–
Adduction	–	30°	–	–

^aCoupled with PIP

2.1.2 Actuators

Each finger in the *DLR Hand I* has four DoF but is commanded only via three actuators, as the DIP is passively coupled to the PIP. The actuator for the interphalangeal joints is located in the proximal link. Table 2 provides the range of motion for each joint. To fit the maximum diameter of the proximal phalanx, the finger joints are actuated by specially designed linear actuators. Each linear actuator consists of a combination of a brushless DC motor with a hollow shaft and DLR's miniaturized planetary roller spindle drive (Fig. 5).

The cylindrically shaped actuators of 21 mm diameter and 33 mm length can apply a maximum force of 150 N. Force transmission is performed using the Dyneema tendons (SPECTRA). However, tendon transmission created some issues, especially related to tendon slack, creep, and overload, as well as reduced lifetime. The drive electronics, the sensors and sensor electronics, are all integrated into the modular fingers. Within the palm, a separated control board provides communication to the external host computer via an optical fiber link. Different teleoperation experiments have been performed with this hand using a data glove and a SpaceMouse as input devices [8]. The controllers for these experiments are run on an external computer.

2.1.3 Sensors

One very effective way to deal with uncertainties in object size, shape, and position is the use of compliance control. Hence, the full state of the hand, consisting of force and position (including their derivatives) has to be known. Therefore, the sensor equipment of a hand plays a central role, and suitable position and force sensors (to be accurate, most force sensors do in fact measure deflection of an elastic body

and, in consequence, a position.) should provide the information required for the control actions.

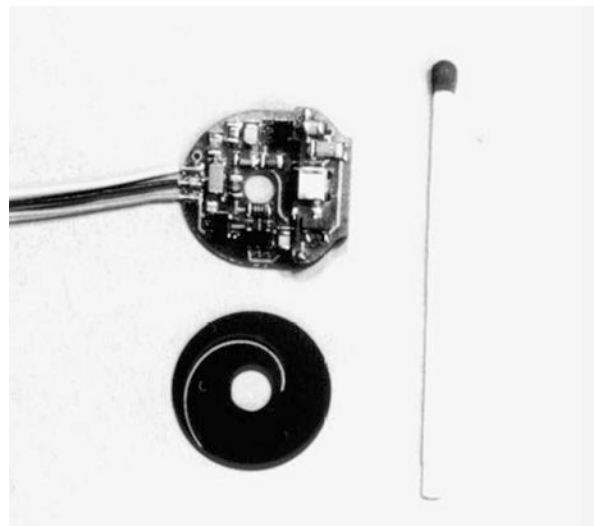
Force Sensors

The force sensors of the *DLR Hand I* are conventional strain gauge-based torque sensors. The force sensors were designed as simple beams located as close as possible to the corresponding axis. The beam located at the medial joint is equipped with two strain gauges to allow for temperature compensation, whereas the sensors of the proximal and the distal joint use four full bridges to provide force measurement in two directions.

Position Sensors

Since the DLR planetary roller spindle drive is a friction-based transmission, slippage and creep of the tendons has to be detected. Hence, each drive has two position sensors. The motor position sensor is calculated by the motor controller itself using the linear Hall effect sensors of the brushless DC motor. The joint position is measured by an in-house designed optical sensor using an infrared LED, a separation disk with a spiral shaped disk, and a position sensitive device (PSD). The latter sensor comprises the voltage regulator and the analogue conditioning circuit at 10 bit angular resolution, providing a linearity error of less than 1 percent. The sensor is 4.8 mm thick and has a diameter of 17 mm (Fig. 4).

Fig. 4 Optical PSD-based absolute position sensor located in the distal joint of the fingers in *DLR Hand I*



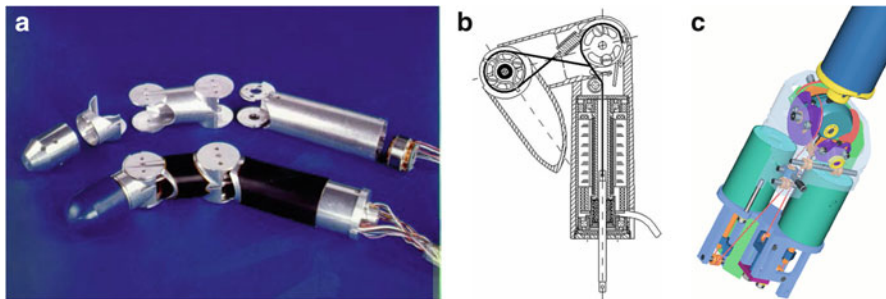


Fig. 5 Mechanical Design of the *DLR Hand I* finger: (a) Finger structure of *DLR Hand I*. The medial and distal axis of the finger are coupled in a ratio of 1:1.05. The black surface is the FSR-based tactile sensor. (b) Cross section of the finger. The pretension of the tendons is ensured by a linear spring. The spindle drive, located in the lowest part of the proximal phalanx, is actuated by a brushless DC motor. (c) basejoint of *DLR Hand I*

Additional Sensors

DLR Hand I was additionally equipped with tactile sensors based on force-sensitive resistor (FSR) to detect the contact location as well as the force magnitude (Fig. 5). To ease up the calculation of the surface normals, all grasping surfaces were made with a cylindrical or spherical shape.

2.2 Results and Lessons Learned

DLR Hand I performed proper grasping of different objects, it was applicable to various robots, and it was a good starting point for the development of dexterous hands with the associated grasping algorithms and control. Nevertheless, the hand showed several weaknesses. At first, the segment lengths of the fingers were unbalanced due to the need to integrate the “artificial muscle.” The short lengths of the medial and distal phalanx led to serious impairments of the hand, in particular when it comes to power grasps or grasps that need the fingertip to get close to the palm surface. This fact was amplified by the too small range of motion of the fingers in the base joint.

In addition, the relatively long finger base (caused by the length of the “artificial muscle”) constrained the placement of the thumb, leading to a “Gorilla-like” thumb placement. The thumb is placed too low in the palm, thus resulting in a poor opposition. This thumb placement is found in gorillas and other primates that mainly perform power grasps, but it drastically reduces the fine manipulation capabilities [48].

The second major issue was the reliability of the hand. In particular, the tendons were a limiting factor, since the small pulley radii and the high loads lead to high tendon wear and breakage.

In terms of sensor equipment, the tactile sensors showed to have some limitations as well. The small bending radius of the FSR led to internal pretension in the sensors, thus producing signals close to the saturation level. Additionally, the surface of the fingers showed to be too slippery and too rigid to ensure proper contact with the object.

3 DLR Hand II

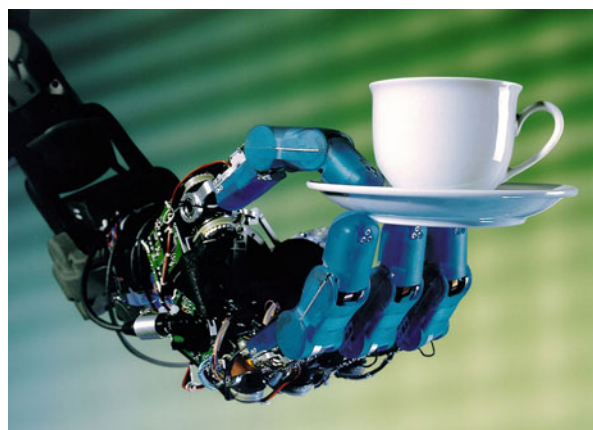
DLR Hand I described in Sect. 2 was a major step toward a dexterous multi-fingered hand that could be used on a rather arbitrary robot. Nevertheless, it had some major issues that limited the use of the hand as a development platform for grasping algorithms and demonstrations. Hence, a major redesign of the hand was started in 1999. The goals set for the development of the previous version were still valid for the new design. The new *DLR Hand II* (Fig. 6) was additionally supposed to:

- Be 50 % faster
- Be able to exert a maximum fingertip force of 30 N (with a fully stretched finger)
- Provide a larger overlap of the finger workspaces
- Be able to perform both, power grasp and fine manipulation
- Be able to perform power grasp of small objects, as well as contacting the palm with the fingertips
- Be reliable

3.1 Design

The design of this hand was mainly driven by the need to improve the reliability and performance of the hand. Since two contradicting goals (getting faster and stronger)

Fig. 6 *DLR Hand II* in its first version. The thumb is located much closer to the finger bases than in *DLR Hand I*, leading to a more natural grasp for fine manipulation



had been set for the design, only a paradigm shift in terms of actuation could solve the problem. Rather than improving the drive efficiency, the actuation concept itself was changed. The abduction/adduction movement of the finger in most cases is used to reposition the fingers rather than to exert significant forces. A quick check of human anatomy shows that, in fact, in the human hand this motion is performed by the rather small (in comparison to the muscles performing extension and, in particular, flexion of the finger) interossei muscles located in the palm of the human hand, which is a strong indication that the forces needed are one order of magnitude smaller than the ones required for extension/flexion.

This consideration left two choices, either using one smaller motor for the abduction/adduction motion and a larger one for the flexion/extension motion, or using a coupled actuation for both axes to allow for using both motors to exert forces in extension/flexion direction. Since a coupled motion also reduces the complexity of the transmission from the motors to the joint, (the transmission actuating the second axis either has to surpass the first axis, or the motor has to be located between the first and the second axis, or even in the proximal phalanx, thus leading to a bulky design.) it was the concept chosen for the new hand. To overcome the reliability problems of *DLR Hand I*, the tendon transmission was replaced by a belt transmission [9].

3.1.1 Kinematics

The kinematics is the most important point in hand design. Hence, additional effort was put into improving the kinematics of this new model. In particular the location and orientation of the base joint as well as the finger kinematics were carefully investigated.

Palm Kinematics and Finger Base Positions

Rather than having one configuration that would allow fine manipulation as well as power grasps (which turned out to be far from optimal for both types of grasps), a simple mechanism was designed to enable synchronous relocation and reorientation of the thumb as well as the ring finger (Fig. 7). To design the joint locations and linkages, two configurations, one for fine manipulation and one for power grasp, were set up in a simulation environment and used for teleoperated grasping using a Cyberglove. An optimization algorithm was used to find an optimal mapping of the end positions of the mechanism to the desired hand configurations using a single actuator.

Finger Kinematics

To improve the fine manipulation performance of the hand and its ability to grasp small objects, three points of interest were determined. At first, the length of the finger base (metacarpal bones) had to be reduced as much as possible to allow a smaller distance between the thumb base and the finger bases. Second, the length of the proximal phalanx had to be reduced to better approximate the proportions of the human hand to allow for better wrapping of objects. Thanks to this design the fingertips could touch the palm, thus enabling power grasps of small objects

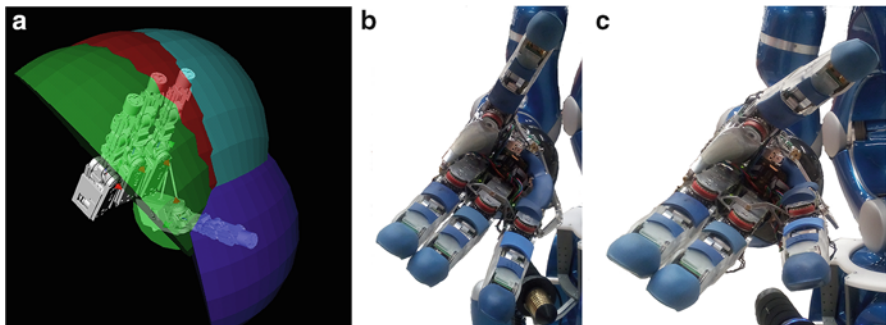


Fig. 7 *DLR Hand II* workspace and configurations: (a) workspace overlap of the fingers (b) hand setup in power grasp configuration (c) precision grasp configuration

Table 3 Finger link length of *DLR Hand I*, *DLR Hand II*, and human middle finger as reported in [7]. The proportions of the phalanges of *DLR Hand II* are much closer to the human ones

Phalanx	Overall	Proximal	Medial	Distal
Length <i>DLR Hand I</i>	173.35 mm	97.35 mm	40 mm	36 mm
Relative ratio	1	0.56	0.23	0.21
Length <i>DLR Hand II</i>	155 mm	75 mm	40 mm	40 mm
Relative ratio	1	0.48	0.26	0.26
Length human hand	92.25 mm	44.6 mm	26.3 mm	17.4 mm +3.95 mm (tissue)
Relative ratio	1	0.48	0.29	0.23

without using the thumb. For this last application, also the range of motion during finger flexion has to be greater than 90°. Like in *DLR Hand I*, this was achieved by tilting the base of the proximal phalanx with respect to the base joint. The tilting angle is 23° for the second revision of the hand. The coupling of the PIP and DIP joint was adjusted to 1:1 to facilitate kinematic calculations (Table 3).

3.1.2 Actuators

The hand uses off-the-shelf brushless DC motors (24 mm diameter at the joint base, 19 mm at the proximal phalanx). In contrast to *DLR Hand I*, all the motions in this version are rotational, to reduce losses in the transmission. The base joint motors drive a harmonic drive gear, each one connected to a belt drive. Each belt drive runs one of two opposing bevel gears. A third bevel gear oriented 90° with respect to the input bevel gear axis is directly connected to the proximal phalanx. The fourth one is a free-running bevel gear that helps to balance the loads on the output bevel gear and enables omitting any bushings or bearings for the second axis of the base joint. All bearing loads are carried by the teeth of the bevel gears. The latter allows for a hollow axle in the output bevel gear to run the cables toward the proximal phalanx (Fig. 8a).

In contrast to the base joint, the belt drive of the PIP joint is located on the low torque side of the harmonic drive gear to allow for a shorter drive unit as well as a

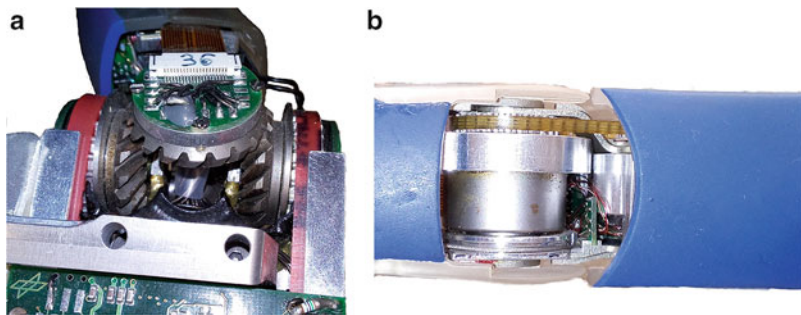


Fig. 8 Drives of *DLR Hand II*: (a) bevel gear setup in the MC joint. The fourth bevel gear (*back*) is free-running and replaces the bearings of the joint axis to allow for a hollow shaft to hold the cables running toward the finger (the cables are running through the center of the PCB in the front and are soldered to the finger connector). (b) PIP joint setup. In contrast to the MC setup, the motor (partially visible on the right-hand side of the belt) is not coaxial with the harmonic drive gear, and the belt drive is running on the low torque side of the gear, thus allowing for more precision and a smaller length of the joint by using a smaller belt

smaller belt (Fig. 8b). The coupling between the PIP and the DIP joint was designed using a pair of steel cables, as well as a tiny tensor on the DIP pulley.

The reconfiguration of the palm is driven by a 12 mm diameter Maxxon brushed DC motor running a threaded rod. The nut running on the threaded rod is connected through a linkage to the base joint of the thumb and to the base joint of the fourth finger. This is not used as a controlled drive, since it just has to run the nut from endstop to endstop to ensure a clearly defined location of the finger base joints in both the precision and power grasp configurations.

3.1.3 Sensors

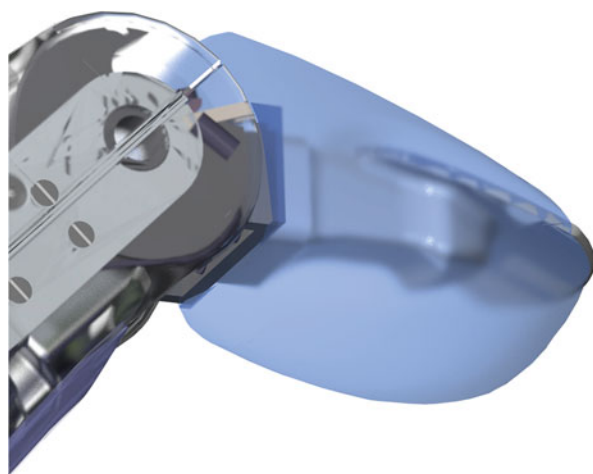
Since impedance control turned out to be the most important feature to achieve proper grasping, a big effort was put into designing position and torque sensors for the finger joints. The torque sensors were designed as strain gauge-based sensors. The sensor for the first two axes was designed as a rectangular beam with strain gauges attached to all four sides of the beam to allow for full bridges and temperature compensation. The PIP sensor was designed as a coaxial sensor using spokes and shear stress strain gauges (Fig. 9).

In the first version, a six DoF force torque sensor was used in the fingertip to measure force magnitude and direction. This allows the estimation of the friction cone and, with a proper control, avoids slippage of the object. During grasping tests, it empirically turned out that having a much softer fingertip is more important for a good grasping performance than directly sensing the contact force and direction. (the contact force now has to be calculated using the measurements of the remaining three joint torque sensors in the finger). Moreover, since the tactile sensors of *DLR Hand I* turned out to have rather poor signal quality as well as being much too rigid

Fig. 9 The PIP torque sensor of *DLR Hand II*. The strain gauges are set up to measure shear stress on the brownish bar of the piece at the right side, which is mated with the groove visible on the Harmonic Drive Gear Flexspline at the left-hand side. The sensor part additionally serves as a pulley for the steel cable-based coupling of DIP and PIP



Fig. 10 Second version of the *DLR Hand II* fingertip. A hammerhead-shaped internal rigid structure supports the shore A 25 PU soft outer hull. The shape of the internal structure – like the human distal plate – keeps the grasped objects from moving distally, and the “fingernail” stabilizes the soft structure in the distal part of the finger pad



and slippery, it was decided to cover the finger pads with soft Polyurethane (PU) skin rather than with tactile sensors.

3.1.4 Skin

The thickness and softness of the finger pads turned out to play a major role in grasp quality. Hence, all grasping surfaces were covered by vacuum-molded housings, providing a soft PU surface. Like in *DLR Hand I*, the grasping surfaces were designed to have a cylindrical or spherical shape to ease up the calculation of surface normals during grasp planning and execution.

For the second revision of the hand, the fingertip was completely redesigned. Inspired by the palmar plate of the human finger, the fingertip consists of a rigid hammerhead-shaped internal structure, covered by a 25 shore A PU soft skin of up to 15 mm thickness (Fig. 10).

3.2 Results and Lessons Learned

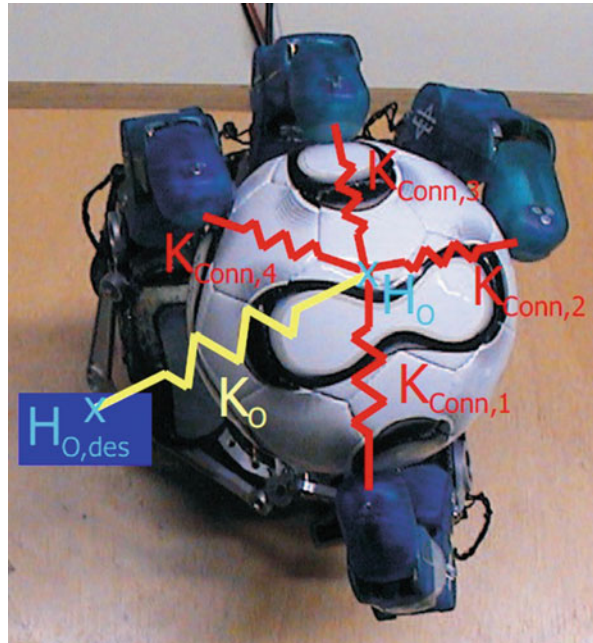
DLR Hand II, after more than 13 years of operation, is still in daily use on the *DLR Rollin' JUSTIN* humanoid robots (Fig. 11) [6], proving that its performance achieved the goals set for the design of modular hands for dexterous manipulation. The control and software architecture of the hand [31] has allowed its usage in teleoperation scenarios with direct control of the hand via a dataglove, and with force and visual feedback to the human operator [10], as well as applications in autonomous experiments such as playing the piano [10] or catching flying balls [2].

Over the years, several algorithmic methods for grasping were developed based on the capabilities of this hand, mainly looking for suitable contact points on the object surface that maximize the resistance to external perturbations according to the analysis in the wrench space [4, 5]. In parallel, suitable control techniques have been proposed to effectively control this type of multi-fingered hands. In particular, the object level impedance controller [61] was proposed to simplify the command of the hand for manipulation tasks (Fig. 12). In this framework, a virtual object (or a virtual frame) is defined within the real object, connected via spatial coupling springs with the fingertips, and connected via an additional spatial spring to the virtual equilibrium position of the hand. By suitable definition of the parameters of this virtual system, the object motion is realized by a corresponding object impedance that generates forces to drive the object from the current to the desired frame. This approach nicely controls the position and internal forces applied on

Fig. 11 *DLR Hand II* has been used in the hands of the *DLR Rollin' JUSTIN* for more than a decade, and they are still in operation



Fig. 12 Passivity-based object level impedance controller used for grasping and manipulation tasks with the *DLR Hand II* [60]; a virtual frame H_O is defined inside the object and connected to the fingertips via virtual springs of constant K_{Conn} . The system is connected via an additional spatial spring to the desired frame $H_{O,des}$



the object but requires always an initial state of contact, i.e., it is not suitable for handling the transition between no-contact and contact. Further extensions of this method allow such transition events, or approach-to-grasp motions, for instance, using finger-to-finger virtual springs [17].

The basic design of the *DLR Hand II* was taken as inspiration for the side developments of two additional hands in cooperation with the *Harbin Institute of Technology (HIT)*. The *DLR/HIT hand I* [41] was constructed as a modular four-finger hand, where each finger had four joints and three actuators, plus an additional motor for changing the relative location of the thumb. This hand had joint position and torque sensors and used commercial brushless DC motors that were integrated in the palm and fingers of the hand. The hand had about 1.5 times the length of a human hand, which was an obstacle for dealing with environments and objects specifically designed for humans. The next generation of this development, the anthropomorphic and modular *DLR/HIT hand II* [16, 42], was constructed with a size comparable to the human hand. It has five fingers, each one with three motors that actuate four joints. However, the thumb has a fixed position relative to the hand, which greatly limits its ability to perform in-hand manipulations [55].

The hands presented so far were developed based on electrical motors and gear-based transmissions. However, for real-world scenarios robustness becomes and is still a key challenge for hand designers. Indeed, hands are the most fragile but most exposed part of any robot. In case of collision, the hand has to carry the whole dynamic load imposed by the inertia of the robot without getting damaged. The next two sections discuss the improvements in terms of robustness for the *Spacehand*,

specifically designed for space applications, and the *Awipi Hand*, designed for withstanding robust interactions with the environment in tasks such as hammering a nail or drilling a hole.

4 Spacehand

The *Spacehand* (Fig. 13) is a multi-fingered robotic hand designed for a multi-year mission in geostationary earth orbit (GEO). It integrates the required actuators, sensors, and computing platform and can be controlled with a joint-level impedance controller. Similar projects are pursued by Jet Propulsion Laboratory (JPL) with the hand of Robonaut [47] or at the University of Laval with the *SARAH* hand [56]. The *Spacehand* is, however, the only multi-fingered torque-controlled robotic hand designed for use in outer space.

The development of *Spacehand* started in 2014 [15], built upon the experience gained with the development of *DEXHAND* [12] (see Fig. 13). Both designs are based on the components of the *DLR Hand II*, improved to cope with the added constraints of a space application, including extended part performance and considerations on radiation tolerance and thermal control. Table 4 summarizes the main qualitative differences with other hands developed at DLR.

The most important change made for *Spacehand* is the reconsideration of the modularization level. Indeed, based on the experience collected through the use of the *DLR Hand II* on *DLR Rollin' JUSTIN*, it was evident that the thumb placement and strength are paramount in achieving a functional hand. Therefore, the *Spacehand* is using a drive-level modularization and a semi-modularization for the fingers. This design strategy allows to reuse as much of the design as possible without diminishing the hand performance.

4.1 Design

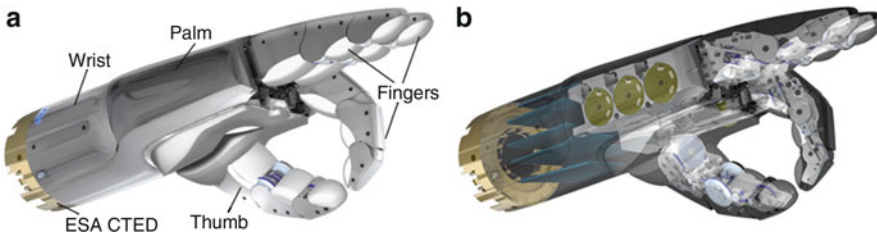
The *Spacehand* has 12 actuated DoF, distributed in four fingers with three DoF each. The electronics are placed in the wrist part, between the mechanical interface to

Fig. 13 *DEXHAND*, a self-contained hand developed for space applications



Table 4 General qualitative comparison of the DLR hands

System	Modularity level	Environment
DLR Hand II	Fingers	Laboratory
Awipi Hand	Actuators	Laboratory
DEXHAND	Actuator modules, special thumb	LEO for 6 months
Spacehand	Actuator modules, special thumb	GEO for several years

**Fig. 14** Spacehand: (a) overall structure; (b) internal architecture

the arm and the fingers (Fig. 14a). The actuation system is based on geared motors followed by a tendon transmission system (Fig. 14b). Joint torque measurements are available and realized with full-strain gauges bridges. Numerous temperature probes and heating foils are available to protect the system against overheating or freezing. The hand is powered by two independent electrical circuits, one for the heating power supply and one for the system itself. The required power for operation oscillates between 20 W and 100 W, depending on the speeds and torques of the joints.

The system is controlled by using a powerful combination of a floating point digital signal processor (DSP) and a field programmable gate array (FPGA). The control system of the hand is running entirely inside the hand. Indeed, although the Spacewire bus used for communication would provide enough bandwidth for high-performance external impedance control, the internal control avoids the burden of integrating the hand controller into the spacecraft control architecture. The communication from the base station to the hand is relayed by several antennas with high bandwidth but high latency.

The shielding strategy consists in housing the whole electronic system in an aluminum shell of at least 2 mm thickness (which is conductive). It serves multiple purposes: as electronic shield for absorbed and radiated emissions, as a radiation shield, and as a thermal conductor, to distribute the heat in the hand. This fully sealed hand body contains the drives, the power electronics, and the communication electronics. The only exceptions are the torque sensors, based on strain gauges, and some temperature sensors, which must be located in the fingers.

4.1.1 Mechanical Structure

In the *Spacehand*, a modular design for the fingers is used in order to increase the system reliability and to allow the finger units to be tested and calibrated before

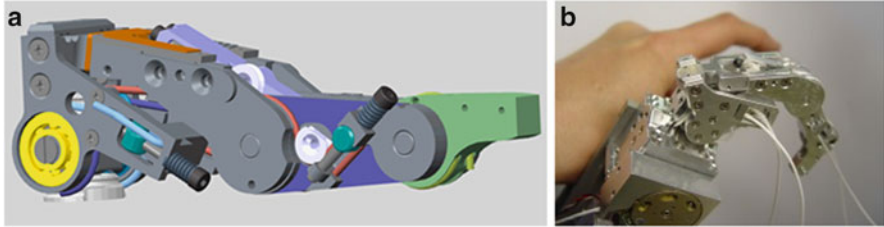


Fig. 15 Finger of *Spacehand* without housing

being assembled in the hand. Figure 15 shows a finger module without housing. However, based on a kinematic analysis and the experience from the *DLR Hand II*, the thumb deserves a special treatment in order to increase the hand dexterity. For example, in order to properly oppose to the other fingers, the thumb should have at least twice the fingertip maximum force. Thus, *Spacehand* fingers are designed to actively produce a fingertip force of 25 N while withstanding 100 N passively.

The transmission system uses Zylon tendons (a high-strength polymer) and harmonic drives in order to bring the torque of the motors to the joints. The concept keeps the electronics of the fingers to a minimum, to improve shielding. Similar to *DLR Hand II*, the cardanic MC base joint is driven by two motors in a diagonal configuration. This diagonal configuration introduces a coupling such that the base joint flexion/extension (resp. abduction/adduction) is achieved by moving both motors with the same speed and direction (resp. same speed but different directions). The tendons used to drive the PIP are routed around the base joint and have therefore a coupling with the base. That is, flexing the finger without flexing the PIP requires a motion of the PIP motor. The PIP joint has a fixed coupling with the DIP with a ratio of 1:1, such that a PIP flexion automatically flexes the DIP.

The relation between motor velocity $\dot{\theta}$ and joint velocity \dot{q} is given by $\dot{\theta} = P\dot{q}$, where P is a coupling matrix given by

$$P = \frac{1}{r_p} \begin{pmatrix} r_1 & r_2 & 0 \\ -r_1 & r_2 & 0 \\ r_{13} & r_{23} & r_3 \end{pmatrix} \quad (1)$$

with r_p being the motor pulley radius; r_1 , r_2 , and r_3 are the joint pulley radius; and r_{13} and r_{23} are the pulley radius of the PIP tendons in the base. Given that the coupling matrix is not configuration-dependent, the relation between motor position and joint position q can be obtained as $\theta = Pg$. Since the structures of fingers and thumb are functionally identical, an automated setup has been developed to systematically verify the fingers. It allows the detection of any deviation in performance and minimizes the time required for hand assembly. It also improves the cost efficiency of the project.

4.1.2 Motor Modules

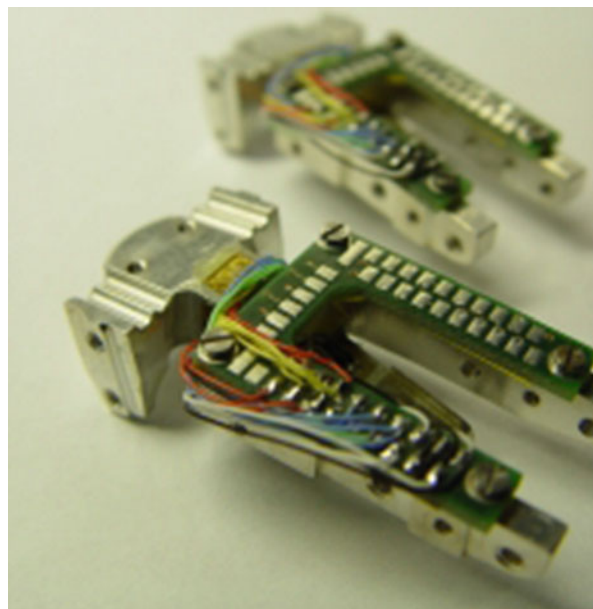
The motor unit for *Spacehand* has been developed based on the DLR/Robodrive (<http://www.robodrive.com>) ILM 25 motor paired with a harmonic drive HFUC 8 with a transmission ration of 100:1. The unit fits into a cylinder of 27 mm diameter and a length of 17.5 mm, with a weight of 46 g. One important lesson learned from *DEXHAND* was that the motor cable, which was directly soldered on a PCB in the back of the motor, was fragile and required utmost care when assembling the fingers. Therefore, the *Spacehand* motor modules integrate space-grade connectors, thus ensuring an easy manipulation of the motor modules during assembly. The unit provides a continuous torque of 2.4 Nm with peaks up to 9 Nm, which is the maximum peak torque of the gearing. In the *DEXHAND*, the motor has been electronically limited to 2 Nm for power reasons (specifically, to limit the maximum current).

4.1.3 Sensors

The joint torque measurement is implemented using a sensing body and a full-strain gauges bridge (Fig. 16) of 5 k Ω sensors. Special care was given in the design of the body sensor in order to prevent temperature drift. The force measurements obtained in a thermal chamber from -50° to 70° confirmed the measurement stability. The torque sensors are all physically located in the proximal finger link; therefore, the sensor for the PIP and DIP joints measures the reaction torque of the coupling tendons.

Each actuated joint has a reference sensor at the end of its motion range. The sensor consists in a small magnet and a Hall effect sensor located in the actuated

Fig. 16 Body of the torque sensor in *Spacehand*



joint. At system power on, a referencing procedure can be executed to obtain the absolute mechanical position of the joints. Reading the state of the sensor directly indicates the direction in which the joint should be moved until the sensor triggers (either a falling or a rising edge depending on the initial state).

4.2 Results and Lessons Learned

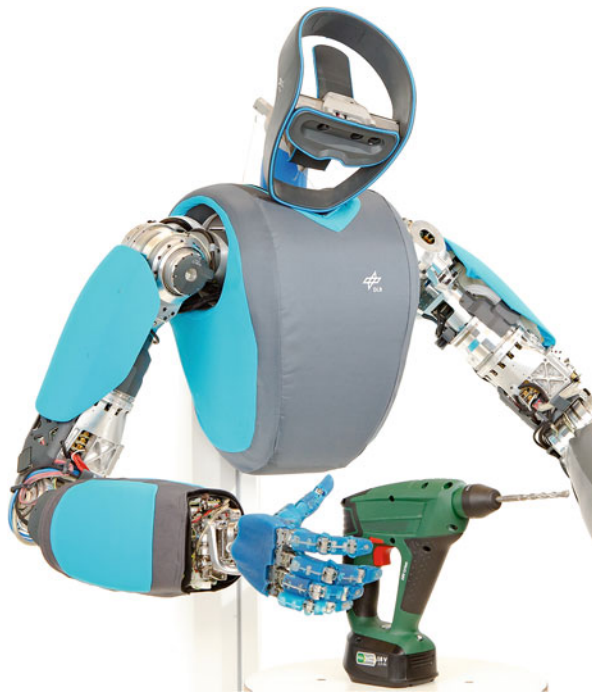
In contrast to its predecessors *DLR Hand I* (Sect. 2) and *DLR Hand II* (Sect. 3), the *Spacehand* did not use the concept of self-contained fingers. On the downside, this modularization concept on drive level (rather than on finger level) does not allow anymore for start-up operations or debugging and maintenance of single fingers, but this turned out to be a minor issue, since all these tasks can be done on motor unit level as well. Furthermore, it is not possible to change complete finger units within a couple of minutes like in *DLR Hand II*. Nevertheless, the semi-modular design of the finger units still allows to change a finger in a reasonable amount of time (but due to the very good reliability of *Spacehand*, changing a finger is rarely done.) But on the other hand, the new modularization concept allowed for much more flexible design of the kinematics of the hand and, in particular, the thumb. During the operational tests of the *Spacehand*, the hand turned out to have a grasping performance that is by far superior even to *DLR Hand II*. The modularization concept of the *DEXHAND* and the *Spacehand* will be the basis of the next modular hands designed at DLR.

In terms of reliability, the hand successfully passed all necessary qualification tests (the full set of qualification tests for space certification has not been performed yet, but all major pretests are done.) and currently the flight-like engineering model (where all parts are fully replaceable by the radiation hardened flight parts, which are one order of magnitude more expensive). for an on-orbit servicing mission is prepared and will be followed by the flight model within the next two years.

5 Awiwi Hand

Building and using two generations of modular hands over a period of more than ten years, it became clear that robustness against impacts is a major issue in robotic hands. Indeed, in service robotic applications the hand is the most exposed part of the robot, even though it is designed for relatively small forces (typically a few Newtons). Furthermore, robotics evolved from lab environments toward more realistic and hard to predict or unknown environments, making collisions with other objects inevitable. In real applications, it is of paramount importance for a robotic system to successfully and reliably complete its task. It needs to be able to withstand collisions and impacts without suffering severe damage or functional impairment [27, 29, 30]. Note that in highly structured environments, the maximum velocity of most robotic hand-arm systems is limited by the ability of the hand to withstand impacts [28]. Additionally, robotics has moved toward working on environments

Fig. 17 DLR's humanoid robot upper body *David*, based on the *DLR Hand Arm System*, an anthropomorphic hand arm system using variable stiffness actuation developed at DLR. It is intended to approach its human archetype in size, weight, and performance. The focus of the development is on robustness, dynamic performance, and dexterity [29]



that are built for humans, which requires advanced physical human robot interaction (PHRI). These environments demand human-sized and human-shaped hands to allow manipulation of human-intended objects, including for instance tools, as well as to improve predictability and acceptability in PHRI [30].

The requirements mentioned beforehand led to the development of the *DLR Hand Arm System* (Fig. 17). The *DLR Hand Arm System* has proven to be an order of magnitude more robust against impacts than previous designs, and about 2.6 times faster than *DLR Rollin' JUSTIN* [62], which is already fast enough for applications such as catching and throwing balls [1]. The system is even capable of withstanding the impact of a baseball bat in full operation without being damaged or even decalibrated [63].

This step forward toward robots with humanlike performance was achieved by introducing the ability to store energy in elastic elements, like in the human archetype (humans have the ability to store a significant amount of energy in muscles and tendons), and by this achieving dynamic decoupling of the link and the drive train.

5.1 Motivation and Goals

DLR Hand I and *DLR Hand II* have been a very good basis for grasping developments at DLR for many years, and *DLR Hand II* is still under heavy use

on *DLR Rollin' JUSTIN* in lab environments. But to tackle the challenges of “real-world” environments, a step toward more anthropomorphic rather than humanoid hands is needed. To the authors’ belief, humanoid appearance is just a subset of the characteristics a robot hand should share with the human being. A hand for a humanoid robot should have the most important characteristics of the human archetype and, by this, be *anthropomorphic* (*anthropomorphic*: “the attribution of human characteristics or behavior to a god, animal, or object” [51]) rather than *humanoid* (*humanoid*: “having an appearance or character resembling that of a human” [52]).

Apart from being *humanoid* in terms of shape and size, being *anthropomorphic* includes characteristics of the human archetype that are of major significance in unstructured environments:

- Robustness against collisions
- Fast dynamics and humanlike force properties
- Enhanced grasping performance

The major objective of the design is to apply these *anthropomorphic* characteristics to a human-sized robot hand for the *DLR Hand Arm System*, referred to as the *Awiwi Hand* (*Awiwi*: Hawaiian for fast. The name is inspired by the name of the WIKI hypertext system. The latter is derived from the Hawaiian word wikiwiki and is as synonym for awiwi). The hand was designed sharing the anthropomorphic design principles with the *DLR Hand Arm System*. The drives must be integrated into the forearm to meet the spatial restrictions. Furthermore, the transmission between forearm and hand has to be routed through the palm and wrist, without affecting the wrist’s range of motion.

5.2 Design

This section provides an overview of the design of the *Awiwi Hand*, focusing on the kinematic design, the drive train, the mechanical design of the hand itself, and finally the sensor equipment. In-depth information can be found in [11, 22, 23, 26, 28, 30].

5.2.1 Kinematics

The kinematics of *DLR Hand II* was designed mainly using optimization, and supported by the results achieved when performing telepresent, semiautomatic, and automatic grasping of virtual objects. The experiences using the hand clearly showed that the virtual grasping concept is a very useful tool for grasp analysis and kinematics design, with its own limitations. For example, virtual grasping does not fully support intuition, which is a very helpful criterion for humans [32]. Even nonexperts can easily recognize whether a kinematics performs well by just looking at the hand in motion. The great efforts taken in hand animations used in movies and games exemplifies this ability [49].

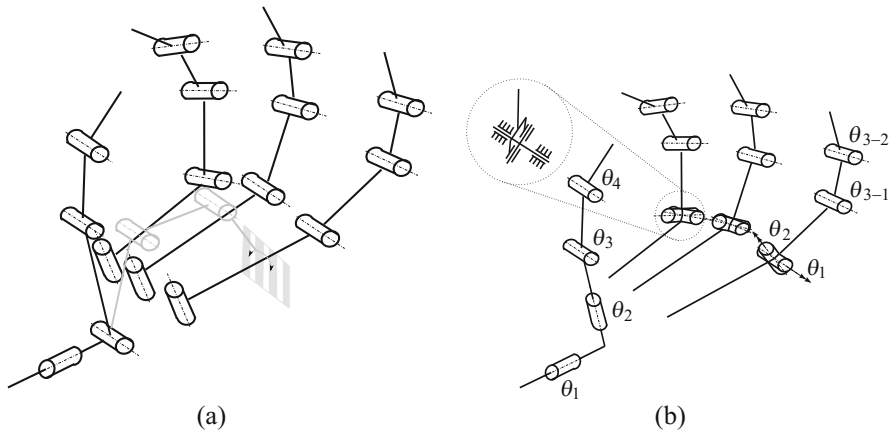


Fig. 18 Reconstructed kinematics for two hands. Joints that are coupled share the first index. (a) UTAH/MIT Hand: The chosen orientation of the first thumb axis is used by several other hands, such as the Twendy-One Hand, and Elu 2 Hand. The gray position of the thumb shows the limitations due to the singularity of the first axis. (b) Twendy-One Hand: The first thumb axis is similar to the UTAH/MIT Hand, but the second joint is a roll joint and avoids the thumb tip singularity close to the index MC. Note that in contrast to the UTAH/MIT Hand, the Robonaut Hand, and most other hands, the first MC axis of the fingers points sideways

Virtual grasping using grasp planners often results in “unnatural motions” (unnatural does not relate to being good or bad in terms of grasping; it just makes the judgment of whether a grasp is intuitive or not), or even in unsuccessful grasps in situations where a human would have successfully grasped by directly operating the virtual hand. Telepresent grasping lacks force feedback, introduces pose errors, and uses too many simplifications to allow for a realistic grasping situation. Consequently, extensive research has been done at DLR on more suitable kinematics design methods, resulting in the insight that a deeper understanding of the human hand on a functional and abstract level is needed. Additionally, an in-depth study of existing hands and their strengths and weaknesses has been performed to derive design guidelines for the *Awiwi Hand*. This design process is summarized here; more details can be found in [26, 30].

Analysis of Existing Robot Hands and the Human Hand

The first step to design a hand kinematics for the *Awiwi Hand* was to thoroughly analyze existing solutions for the problem to be solved, which in the case of the *Awiwi Hand* is grasping and manipulating objects. Both robotic and human hands give valuable hints and guidelines for the design of a new robotic hand [26, 30].

Existing Robot Hands

A large number of robot hands have been built in recent years. For the *Awiwi Hand*, the strengths and weaknesses of several hands were analyzed, in particular with respect to the order and placement of joint axes and placement of joint singularities

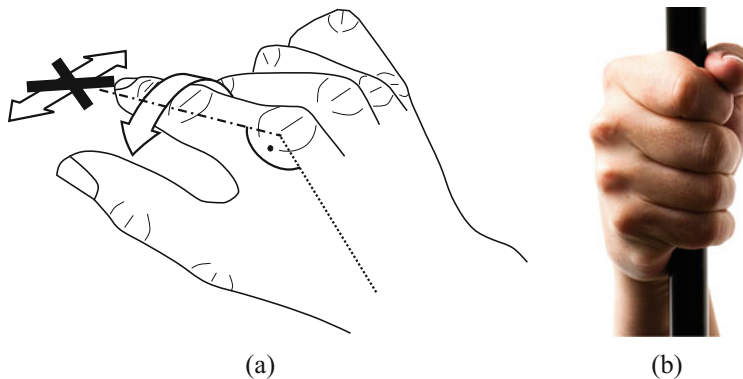


Fig. 19 Motion and functionality of the human MC joint: **(a)** the human MC joint gets in a singular position at approx. 90° flexion. Hence, the finger starts to roll rather than moving sideways. The finger is *structurally* locked against sideway motions in this position. **(b)** This locking is functionally needed to, e.g., climb a pole, since the human hand has no muscles that are capable of providing the loads needed for that task

(Fig. 18), including the UTAH/MIT Hand [37, 38], the Robonaut Hand [47], the UB3 Hand [43–46], the hand of Armar 3 [40, 58], and the Twendy-One Hand [36, 59]. This analysis showed, for instance, that the placement of the first thumb axis and its corresponding singularity is crucial for a good grasping performance [26].

The Human Archetype

The performance of the human hand is by far superior to the performance of current robot hands. Hence, a functional abstraction of its capabilities gives valuable insights on how to design a *good* hand kinematics. An illustrative example of such analysis is the human MC joint. Even though the MC joint of the human hand is a condyloid joint (a ball and socket joint having an elliptical “ball” rather than a spherical “ball”) [25, p. 267][39, p. 176], the range of motion of the human fingers as well as the motion itself (Fig. 19a) show that from a functional standpoint it is a universal joint with the first axis orthogonal to the palm plane. The resulting singularity provides the functionality to lock the fingers’ sideways motion, which enables the human to perform actions such as climbing a pole (The muscles driving abduction and adduction are by far too weak to support the loads applied to the fingers in those situations) (Fig. 19).

Kinematics Design

Based on the design criteria derived from the functional analysis of robot hands and the human archetype, prototypes of the hand kinematics were built in cardboard. Inspired by Adalbert Kapandji, these prototypes are easy to build, modify, and use. For fine adjustment, the use of more accurate prototypes as well as computer simulations is recommended. These prototypes were evaluated using different techniques to facilitate further improvements, including:

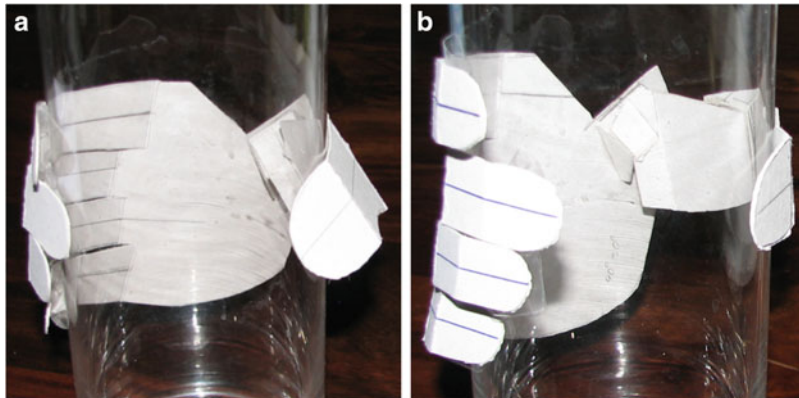


Fig. 20 Power grasp of a large cylindrical flower vase to test thumb joint axis orientation parameters. (a) The thumb with an axis orthogonal to the sagittal plane of the respective phalanx meets the cylinder quite laterally and thus does not bring the frontal pad of the thumb in contact, leading to poor object contact and lateral forces on the joints. (b) The prototype providing non-orthogonal axis (implementing twist and inclination) is in perfect frontal contact to the vase

- Medical tests
- Grasping a set of objects specific to certain grasp types
- Human intuition while using the prototypes

As an example, the orientation of the nonparallel axis of the thumb IP and MP joint, called inclination (inclination: the angle between the sagittal plane with respect to the frontal plane) and twist (twist: the angle between the sagittal plane and the axis with respect to the longitudinal axis of the phalanx) [39, p. 188], largely influences the grasp quality for large cylindrical objects, as depicted in Fig. 20. These parameters have been used to fine-tune the orientation of the thumb pad in flexed and stretched out positions. The final kinematics for the *Awiwi Hand* is illustrated in Fig. 21. For more details, see [11, 26, 30].

5.2.2 Drives and Structure

The *Awiwi Hand* is designed to provide a step change in terms of hand dynamics and robustness. Such objective is only achievable using actuation that provides energy storage mechanisms such as passive elasticities. Furthermore, following the design philosophy of the *DLR Hand Arm System*, the stiffness of the fingers should be adjustable for each grasping situation. In addition, the hand should be of human size and still capable of providing humanlike grasping forces. The latter demands that, like in the human archetype, the drives for the fingers are located in the forearm rather than in the hand. Tendons are chosen to transmit the actuation forces to the hand. With all these bounding conditions in mind, antagonistic actuation was selected for the hand (Fig. 22).

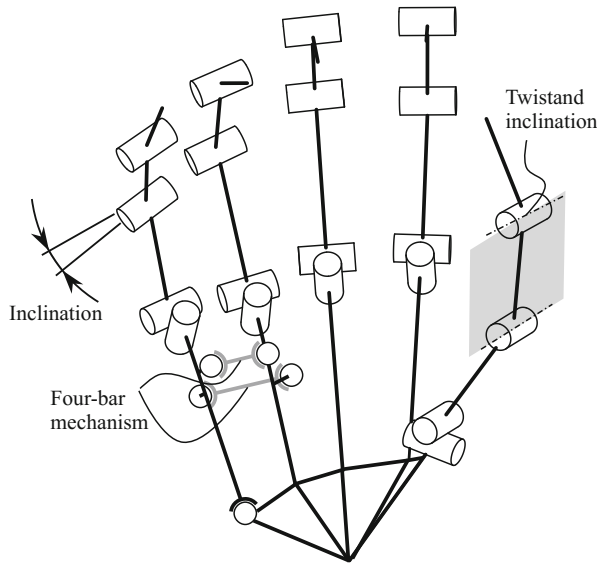


Fig. 21 Kinematics scheme of the *Awipi Hand*. All fingers other than the index and middle finger have inclination in all hinge joints to improve opposition and power grasp of spherical objects. The thumb IP provides inclination as well as twist to compensate the missing fifth DoF of the thumb and improve key grasp and power grasp performance. The MC joints, as well as the thumb TMC, have orthogonal but nonintersecting axes. The little finger HMC is designed as a four-bar mechanism with a spherical joint on the proximal end of the metacarpal. This enables inward rotation of the little finger, as well as palmar motion of the MC joint itself, which arches the palm to locate cylindrical objects of smaller diameter firmly during power grasp

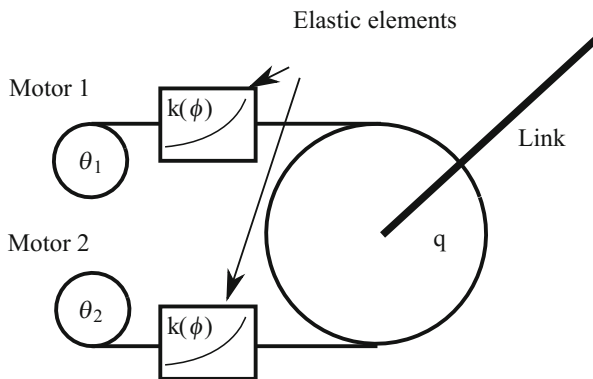


Fig. 22 Antagonistic actuation scheme. The joint is actuated by two motors connected to the link by a nonlinear elastic element with stiffness characteristics $k(\phi)$, where ϕ is the elastic element deflection, θ denotes the motor positions, and q is the link position

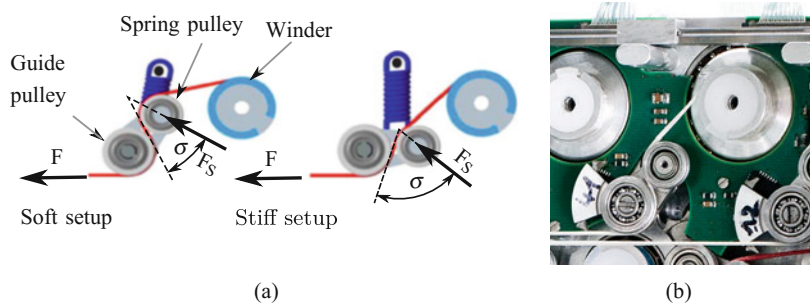


Fig. 23 Antagonistic drive compliance mechanism (“tendon side-pull mechanism”): (a) the pulley located at the spring loaded lever rotates around the center of the guiding pulley and exerts F_S . Due to this design, a nonlinear relation between tendon force and spring elongation is obtained. Low mechanical stiffness is achieved by small σ ; large σ results in high stiffness. (b) Final elastic element design. The winder is located on the upper right

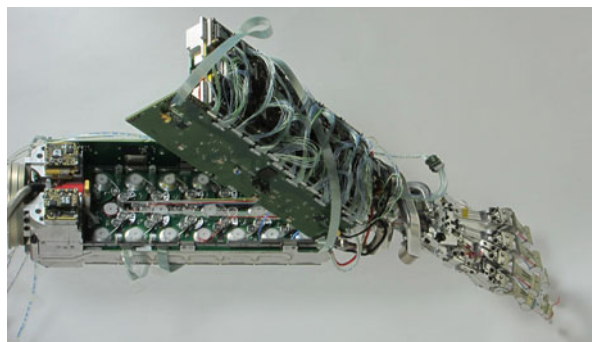


Fig. 24 Split forearm design: the ServoModules are located on the outer part of each half and thus are easy to access. The tendons and elastic elements are located in the middle layer between both halves. This *split design* protects the tendons in the middle of the forearm and enables easy access to the tendons for maintenance. The forearm is fully operational (at limited tendon loads) if open. To replace a ServoModule, only two screws must be removed, and the low level bus connector has to be disconnected

In the forearm of the *DLR Hand Arm System*, 38 drive units are set up symmetrically to the middle plane of the forearm, as depicted in Fig. 23. Each unit consists of a brushless DC motor with integrated drive electronics, a harmonic drive gear, and an elastic mechanism. This setup allows to open the forearm even in operational mode to allow for maintenance and repair (Fig. 24).

The endoskeleton structure of the fingers of the *Awiwi Hand* is depicted in Fig. 25. All the joints are designed as hinge joints (Fig. 26) providing inclination and, in case of the thumb IP joint, twist to enable proper orientation of the thumb pad (Fig. 29). The MC of the fingers as well as the TMC joint of the thumb are

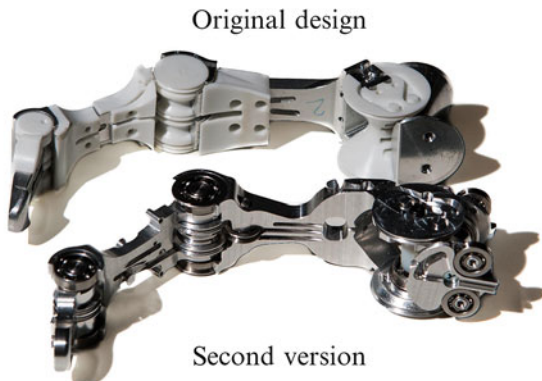


Fig. 25 Endoskeleton structure of the fingers, providing low-component count and abundant space to apply soft pads to improve grasping performance. In the first version [28], the white tendon guidances are made from friction bearing plastics to reduce capstan friction. In the second version [22], the tendons run on ball bearings to reduce friction even more. The tendons of the PIP and DIP joint are routed through equivalent slots in the proximal hyperboloid (Fig. 27)

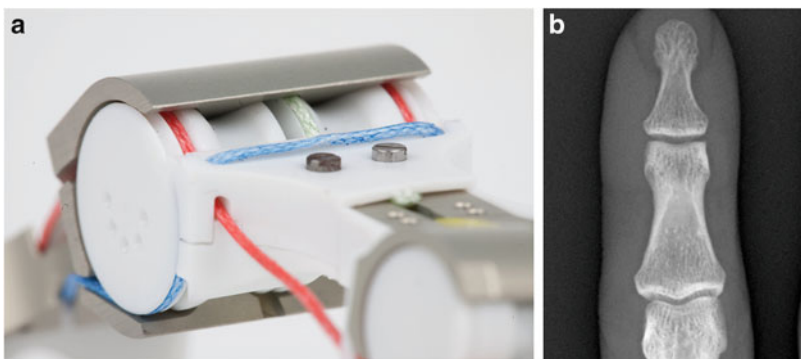


Fig. 26 PIP joint design: (a) the open hinge joint design of the robot finger; (b) its human archetype (index finger). The ridges of both joints keep the joint in place axially. The two PIP flexor tendons (blue) in (a) are routed as far as possible from the sagittal plane of the finger to provide the leverage necessary to withstand lateral forces. The PIP extensor tendon (green) is placed close to the sagittal plane

hyperboloid joints (Fig. 27) providing the motion characteristics of the human joints described in Sect. 5.2.1. Since the forces exerted on the thumb in opposition result from the grasping forces of the up to four opposing fingers, the thumb is set up with significantly larger pulley diameters as well as stronger structure.

To reduce friction in the fingers (in particular capstan friction), the finger joints were changed from sliding friction joints to ball bearings for the second version of the *Awiwi Hand* (Fig. 25), and the Dyneema tendons were replaced by steel cables. Dyneema tendons turned out to have a significant amount of internal friction even

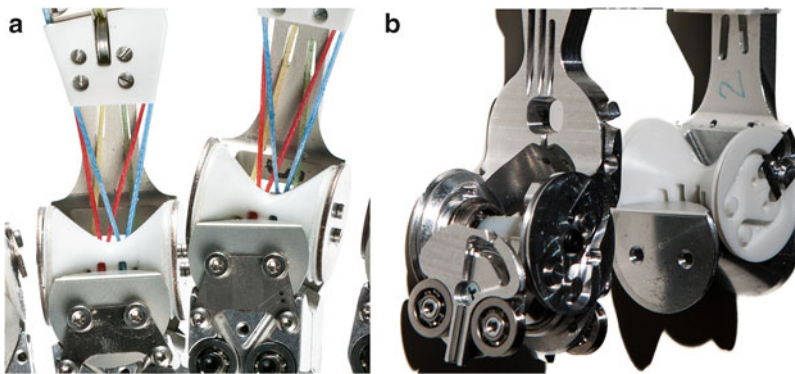


Fig. 27 Hyperboloid-based anthropomorphic MC joint. (a) The hyperboloid shape of the first version reduces the joint friction drastically since, assuming the load is mainly promoted in the center of the joint, the lever of the pulley (white tendons) is much larger than that of Coulomb's friction; (b) the second version of the MC joint combines the hyperboloid joint with ball bearings to reduce friction even further. The hyperboloid surfaces are not in contact under nominal loads

on ball bearing pulleys [23, 54]. Since the maximum load of the bearings as well as of the steel cables constrain the allowable maximum fingertip force, the fingertip forces have been reduced from 30 N to 21 N [23].

The palm has to accommodate all 38 tendons needed to drive the fingers and the thumb. To reduce friction, the 38 tendons are routed toward the fingers using ball bearings (Fig. 28). The palm in the first version also provided a four-bar kinematics to allow for motion of the fifth finger toward the thumb to improve opposition, in particular when grasping small sphere-shaped objects. For the sake of simplicity, it has been omitted in the second version (at the current state of research, fine manipulation is not the main focus) but might be implemented again in future versions. For the second iteration of the palm, even the guidances for the thumb tendons have been changed to ball bearings.

5.2.3 Thumb Design

The human thumb is the most important digit of the human hand [48]. It must be significantly stronger than the other fingers in order to be able to oppose multiple fingers (especially during power grasp) while carrying the loads exerted onto the object by the fingers. Although the human thumb has five DoF [3, 24, 39], the thumb of the *Awiwi Hand* was implemented with four DoF to meet the constraints of the *DLR Hand Arm System* without major functional impairments.

The structure of the thumb is similar to the other fingers but additionally implements twist and inclination to adjust the orientation of the thumb pad in stretched and flexed positions (Fig. 29). To provide enough finger force to oppose two or even three fingers, the pulley diameters of the thumb are larger than for the other fingers.

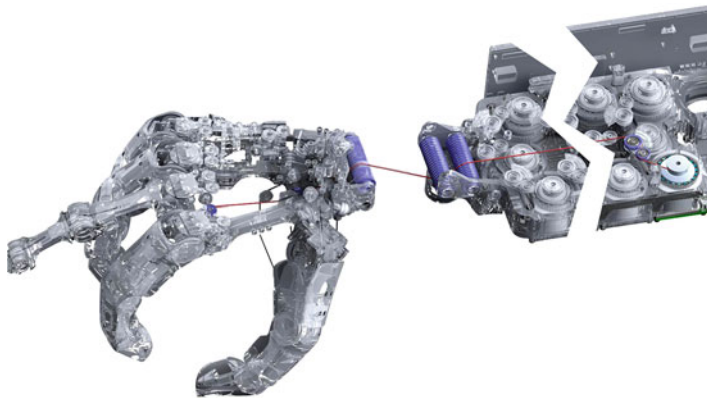
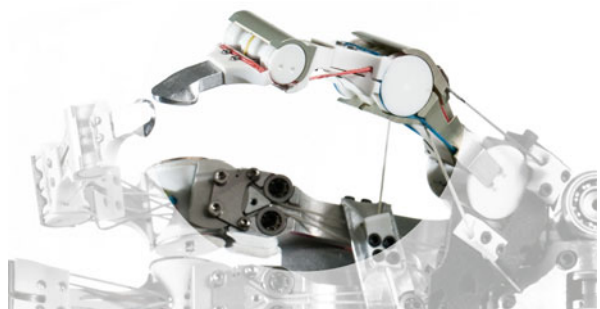


Fig. 28 Routing of a single tendon (red) starting from the winder (right) to the finger joint. The tendon runs over the spring-loaded lever that embodies the elastic element toward the wrist pulleys that guide the tendon into the palm. All direction changes of the tendon in the palm are designed using ball bearings as pulleys [23]

Fig. 29 Twist between the IP and MP joints (inward rotation of the IP axis with respect to the MP axis) for the thumb. It enables the thumb to make a more frontal contact in particular with large cylindrical objects during a power grasp (Sect. 5.2.1)



Since the TMC would be much too bulky in a setup similar to the finger MC, the thumb is actuated by four tendons reaching from the palm to the phalanx in the first version of the *Awiwi Hand* (Fig. 30). This setup provides the desired fingertip force of 40 N, but the controllers have to compensate the nonlinear motion characteristics of the thumb TMC. In the second version of the *Awiwi Hand*, the setup has been changed to a hybrid setup that uses the mechanism of the fingers (tendons on pulleys) for the extensors of the thumb [23].

5.2.4 Design of the Palm

The palm of the *Awiwi Hand* has to direct the tendons from the wrist pulleys (Fig. 31) to the fingers with a minimal amount of friction. Hence, the palm is designed to use ball bearings as pulleys. To improve tendon lifetime, the pulleys are oriented in three DoF to exactly fit the intended tendon pull directions (diagonal pull drastically reduces tendon lifetime and must be avoided when possible). The tendons toward the fingers are routed in three parallel layers to allow for better

Fig. 30 Tendon routing of the thumb. The guidances of the flexor tendons are placed more distant than the extensors to maximize the available tip force, in particular for power grasp. By this, the maximum force at the IP joint location is greater than 80 N. On the other hand, the control of the thumb gets more challenging due to the nonlinear kinematics [13, 14]

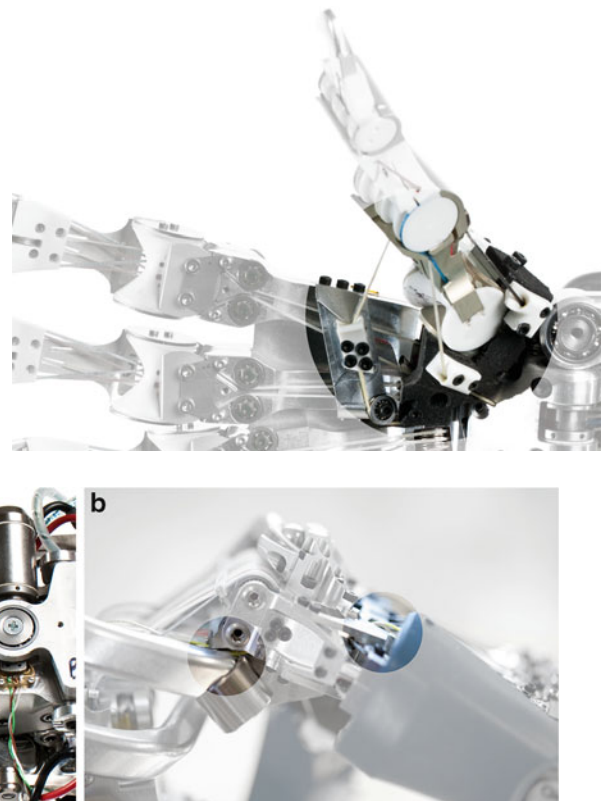


Fig. 31 Tendon routing in wrist and palm: (a) within the wrist, the tendons are guided by pulley arrays on the proximal (forearm) side (right), as well as on the distal (hand) side of the wrist (left). The tendons providing maximum force are placed in the middle of the wrist to reduce (unwanted) torques on the wrist. (b) During maximum flexion, the tendons at the wrist should not lose contact with the pulley array to avoid tendon damage. The yellow tendon (lower left) on the pulley array is routed to the opposite side of the palm (upper right) to prevent losing contact with the pulley

maintenance and assembly. To guarantee secure guidance of the tendons, every tendon is running in a separate groove wherever it was possible. See [26] for more details.

5.2.5 Housings Design

In the human archetype, the tissue and skin of the hand is of major importance for the grasping and manipulation abilities of the hand [48, pp. 29–40, 42–44]. It provides the contact surfaces to the object and locates the object within the hand firmly, in particular when performing power grasp.

The pads of the human hand are a complex combination of the skin, the underlying muscles, and a ligament structure. This ligament structure fastens the skin in order to be able to transfer stress to the skeletal structure (Fig. 32). In

Fig. 32 Example of stress distribution functionality of the skin: a Fakir [53]. The contact pressure at the nails would easily damage the underlying structures, such as nerves, veins, and muscle fibers without the stress distribution functionality of the skin



Fig. 33 Hand with housings, consisting of rigid parts transferring the stress to the structure, and a thick soft polyurethane skin. The housings do not cover the joints themselves. The transition between palm and thumb is fully flexible to improve power grasp performance



contrast, it also allows for a direction-dependent range of motion of the skin with respect to the hand skeleton [26].

As with the hand design itself, it is not possible to copy the human *housings* due to the high complexity and the large gap between biological and current engineering technology. The housings of the hand must be designed to:

- Provide high friction for a majority of surfaces.
- Avoid contact of rigid and stiff parts of the hand with the object to prevent damaging the object.
- Adapt to the object shape and thus achieve form closure by the soft skin.
- Locate the object firmly by the housing geometry.

For the *Awiwi Hand*, rigid housings with soft surfaces have been chosen. Every segment of the fingers, the thumb, and the palm has a separate housing, as shown in Fig. 33.

5.2.6 Sensors

Due to the antagonistic drive concept, all states of the fingers can be measured using position sensors. Every drive is equipped with a magneto-resistive position sensor. Another magneto-resistive sensor measures the angular position of the spring lever arm. Using the calibrated nonlinear spring characteristics of the lever arms, the exerted forces on the tendons are calculated, resulting in data for the internal forces (pretension) as well as exerted forces at the fingers. More details are presented in [22].

The second version of the *Awiwi Hand* additionally provides an optional Hall-based joint position sensor to allow for more accurate positioning of the joints, as well as for compensation of tendon creep. More details are provided in [23].

5.2.7 Control

According to the experience gathered with the different robotic hands, the most desirable user interface is a joint-level impedance controller. One particularity of the system, with respect to most similar designs, is that the joints have a redundant actuation. Indeed, as long as the pulling constraints of the tendon are satisfied, each motor is able to increase or decrease the joint torque independently. Consequently, considering only a single joint, the controller has three inputs: the desired joint position, the desired mechanical stiffness, and the joint impedance controller parameters, and the two outputs are the torques for the two antagonists. The available measurements are the spring mechanism positions and the motor positions. From those measurements, the tendon forces, the joint position, the joint torque, and the joint mechanical stiffness can be computed. However, due to the tendon routing, the joint does not allow for any arbitrary stiffness value and must be complemented by an active impedance controller to increase the compliance range. The effective impedance perceived at the fingertip results from a combination of the mechanical stiffness and the controller stiffness. Unsurprisingly, the experience with the platform showed that selecting the values is difficult for the users and eventually, only a few discrete settings are used: soft, regular and stiff based on the task, e.g., exploration or manipulation.

Whereas the presence of springs in the path of the tendons greatly improves the robustness of the fingers and provides a measurement of the tendon forces, it simultaneously introduces a nonlinear coupling between the dynamics of the joint and the dynamics of the motors. Inspired by the mechanical structure and the previous system, the first approach was to use a cascaded control approach where an inner loop maintains the tendon pretension and the joint torque, while an outer loop prescribes the reference torque for the joints, e.g., to achieve a desired joint impedance behavior. Unfortunately, this cascaded approach, successfully used in many robotic designs, has a low performance when applied to the fingers of the *Awiwi Hand*. Indeed, a cascaded controller relies on the time scale difference between the link-side dynamics and the motor-side dynamics, which is only marginally valid in the *Awiwi Hand*. The assumption may very well hold for a given set of control gains and stiffness settings but is not necessarily applicable across the complete stiffness range. A possible improvement takes inspiration from

methods in aircraft control and guidance systems. The equations of the system can be linearized at multiple working points, and the appropriate set of gains can be selected. This method has the drawback of requiring a careful implementation to avoid detrimental effects related to the gain switching. A further extension where the gains are computed online via an optimization procedure has the major drawback of requiring a tremendous computing power. Moreover, since both methods are based on a linearization of the equation, only weak conclusions can be drawn regarding the global stability of the control loop.

Rather than ignoring the nonlinear components, an alternative approach consists in explicitly accounting for the motor dynamics and considering the system as a higher-order differential system. A wise choice of variables and decoupling terms is required to transform the system into two independent triangular differential systems for which several control topologies are available. It is then possible to systematically construct a controller, for example, with the “integrator backstepping” method. Obviously, the equations of the controller contain high-order derivatives that must be carefully handled, either by introducing filters, by using model-based calculations, or by simply neglecting them.

The discussion focused on the control of a single joint, but the control structure is extended to a complete finger by canceling the link-side dynamics or, more simply, by ignoring the link-side coupled dynamics, which is extremely small with respect to the other sources of error. The possibility of adjusting the mechanical stiffness is a new degree of freedom for the planning and the grasp execution. Approaches that minimize the action of the active stiffness might significantly decrease the power requirements. A “good” choice of the couplings and the spring characteristics can also improve the natural behavior of the fingers and greatly reduce the required control action.

5.3 Results and Lessons Learned

The *Awiwi Hand* is the most advanced and complex robotic hand DLR has ever developed. This section presents several tests used to verify the satisfaction of the design goals (Sect. 5.1), as well as the conclusions obtained from the *Awiwi Hand* design.

5.3.1 Robustness

The hand has proven to be robust against impacts in impact tests (Fig. 34a). However, robustness of the hand itself, from a task perspective, is not an important goal. From a task level point of view, the task should be completed even in case that the grasped object collides with the environment. Hence, the robustness of the *Awiwi Hand* grasp has been proven by performing an impact test with a 750 g steel pendulum at a velocity of 4 m/s (Fig. 34b) [26].

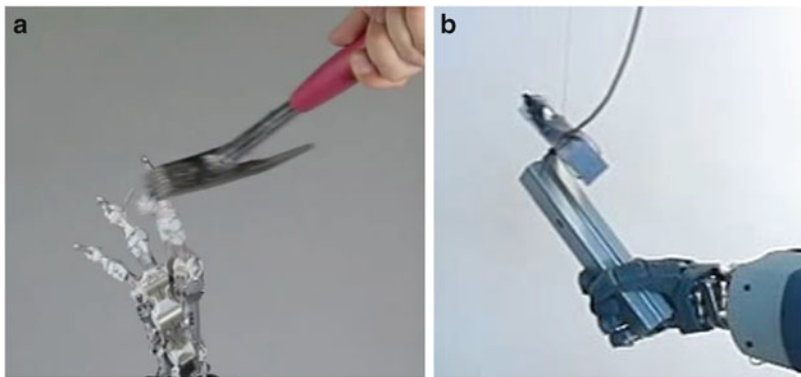
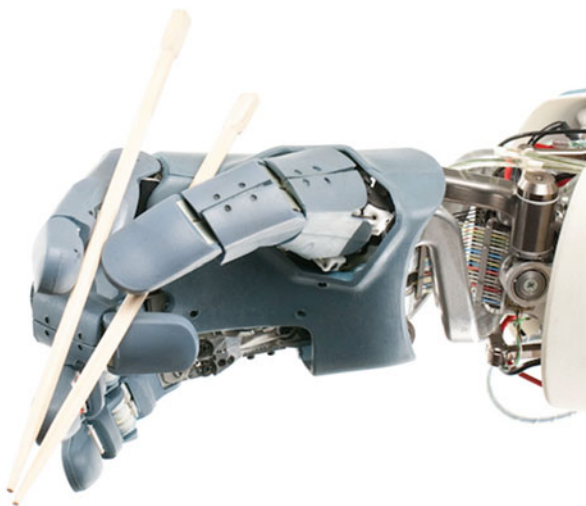


Fig. 34 (a) the *Awiwi Hand* being hit by a 500 g hammer at full operation. The resulting maximum angular fingertip velocity of 3500 °/s would have seriously damaged the hand without the energy storage capabilities of the antagonistic drives. (b) Grasp robustness tests of the *Awiwi Hand*. The hand firmly holds the object being impacted with a 750 g steel pendulum at a velocity of 4 m/s without any damage

Fig. 35 The *Awiwi Hand* grasping chopsticks, one basic and challenging grasp of the taxonomy presented by Feix [21]



5.3.2 Grasping Performance

To evaluate and compare the grasping performance of the *Awiwi Hand* with other hands [19], the *Awiwi Hand* performed all tasks of the *Cutkosky* taxonomy [18] as well as those of the more advanced *Feix* taxonomy [20,21] (Figs. 35 and 36), which has been a first in humanoid robotics according to the authors' knowledge [26].

5.3.3 Lessons Learned

As mentioned beforehand, the *Awiwi Hand* has been revised in some points. On the one hand, the fingers showed a hysteresis due to friction much larger than

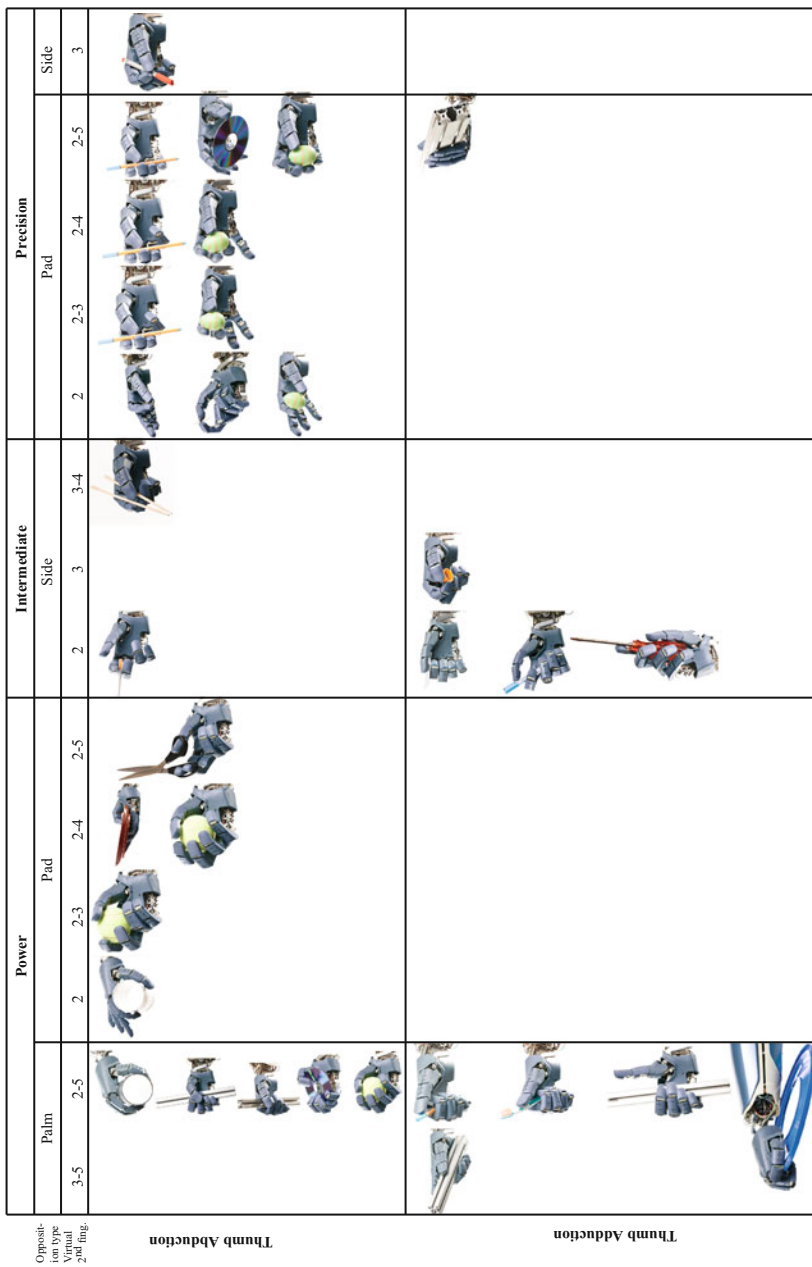


Fig. 36 Feit's taxonomy grasps [21] performed by the *Awipi Hand*. The hand could perform 100% of the taxonomy grasps, which is a first in humanoid robotics. Please note that the grasps have been manually tuned, since current state of the art grasp planning is not capable of performing these grasps

expected and calculated. Within the calculations, the friction of the tendons on the pulleys with ball bearings has been neglected. Thorough investigation of the occurring friction has shown that Dyneema tendons indeed have plenty of *internal* friction on these pulleys, as described in [54]. To regain the aimed functionality of the hand, the tendons were changed to steel tendons, and the fingers incorporated ball bearings in the joints, as described above. This illustrates that the modeling and understanding of tendons and their guidances is an underestimated and not yet completely accomplished task.

On the other hand, the *Awiwi Hand* provided functionalities – such as the articulated HMC joint – that cannot be fully exploited by current state of the art grasping software. Hence, the second version was consequently reduced in terms of complexity to reduce maintenance effort, system cost and – last but not least – control effort and dimensionality of the grasping problem.

6 Final Discussion

At the beginning of DLR's developments in multi-fingered hands, the idea was to develop robots capable of grasping at almost the capabilities of the human archetype. But at that point of time, most “robot hands” were parallel grippers having two or three fingers and aimed for industrial applications. The hands clearly were the bottleneck to develop the ability of grasping.

The first hand developed at DLR, the *DLR Hand I*, was a first step toward better grasping, but it turned out that the mean time between failures was a major problem when it came to developing the grasping ability itself. Hence, the second version, *DLR Hand II*, was consequently improved in terms of reliability and kinematics. This fertilized the development of grasping algorithms and lead to remarkable results, e.g., on the humanoid robot *DLR Rollin' JUSTIN*.

The reliability of *DLR Hand II* together with the technical expertise gained from almost ten years of experience using it inspired us to develop *Spacehand*, aimed to be the first multi-fingered dexterous robot hand in space, where reliability is paramount. In terrestrial applications, robotic algorithms as well as hardware have reached a degree of maturity that enables robots to leave the typical lab environments that, in many cases, have been designed for the robot. Using robots in environments that are unknown or even unstructured or unpredictable imposes a new set of requirements for robot hands. These hands have to be designed to be robust against impacts, grasp the object firmly even in case of collision, and, finally, be able to grasp and manipulate a huge subset of the objects that humans handle in their everyday life. On this line, the *Awiwi Hand* has proven to be robust against impacts on the hand or the object, and has achieved a kinematical grasping performance that is close to the human archetype.

On the other hand, it turned out that many aspects of grasping and fine manipulation, including grasping itself, closing the perception-action loop, grasp planning, and grasp control, are a true challenge when it comes to using them on an integrated robot. Each of these research topics has reached a remarkable level of

maturity, but it is the holistic approach, a clever integration of all the subsystems ranging from object recognition over pose estimation, tactile exploration, grasp planning, and grasp control and supervision, that is currently missing. The maturity of the hands in terms of performance and robustness has surpassed the maturity of grasping abilities. Hence, the holistic approach to grasping and fine manipulation (from the authors' perspective, it is questionable whether distinguishing between grasping and manipulation is helpful) has become the number one challenge in robot grasping. Accordingly, hand design is now focusing on hands that fully support the grasping ability development by being as reliable, simple, and cost-effective as possible while providing the *necessary* performance and capabilities. Keeping the requirements of the hands in sync with the maturity of grasping abilities within the lifetime of a hand design is what we think is the key to develop robots that can manipulate objects like the human archetype.

References

1. B. Bäuml, T. Wimböck, G. Hirzinger, Kinematically optimal catching a flying ball with a hand-arm-system, in *2010 IEEE/RSJ International Conference on Intelligent Robots and Systems (IROS)*, pp. 2592–2599. <https://doi.org/10.1109/IROS.2010.5651175>
2. B. Bäuml, F. Schmidt, T. Wimböck, O. Birbach, A. Dietrich, M. Fuchs, W. Friedl, U. Frese, C. Borst, M. Grebenstein, O. Eiberger, G. Hirzinger, Catching flying balls and preparing coffee: humanoid Rollin' Justin performs dynamic and sensitive tasks, in *2011 IEEE International Conference on Robotics and Automation (ICRA)*, pp. 3443–3444. <https://doi.org/10.1109/ICRA.2011.5980073>
3. A. Benninghoff, *Anatomie: Makroskopische Anatomie, Embryologie und Histologie des Menschen; Benninghoff*, ed. by D. Drenckhahn, W. Zenker, vol. 1, 15th edn. (Urban & Schwarzenberg, München, 1994). ISBN:9783541002450
4. C. Borst, M. Fischer, S. Haidacher, H. Liu, G. Hirzinger, DLR Hand II: experiments and experience with an anthropomorphic hand, in *2003 IEEE International Conference on Robotics and Automation*, vol. 1, pp. 702–707. <https://doi.org/10.1109/ROBOT.2003.1241676>
5. C. Borst, M. Fischer, G. Hirzinger, Grasp planning: how to choose a suitable task wrench space, in *2004 IEEE International Conference on Robotics and Automation*, pp. 319–325. <https://doi.org/10.1109/ROBOT.2004.1307170>
6. C. Borst, T. Wimböck, F. Schmidt, M. Fuchs, B. Brunner, F. Zacharias, P. Giordano, R. Konietzschke, W. Sepp, S. Fuchs, C. Rink, A. Albu-Schäffer, G. Hirzinger, Rollin' Justin – mobile platform with variable base, in *2009 IEEE International Conference on Robotics and Automation*, pp. 1597–1598. <https://doi.org/10.1109/ROBOT.2009.5152586>
7. A. Buryanov, V. Kotiuk, Proportions of hand segments. *Int. J. Morphol.* **28**, 755–758 (2010). ISSN:0717–9502
8. J. Butterfaß, G. Hirzinger, S. Knoch, H. Liu, DLR's multisensory articulated hand: I. Hard – and software architecture, in *1998 IEEE International Conference on Robotics and Automation*, pp. 2081–2086. <https://doi.org/10.1109/ROBOT.1998.680625>
9. J. Butterfaß, M. Grebenstein, H. Liu, G. Hirzinger, DLR-Hand II: next generation of a dexterous robot hand, in *2001 IEEE International Conference on Robotics and Automation (ICRA)*, vol. 1, pp. 163–178. <https://doi.org/10.1109/ROBOT.2001.932538>
10. J. Butterfaß, M. Fischer, M. Grebenstein, S. Haidacher, G. Hirzinger, Design and experiences with DLR Hand II, in *2004 World Automation Congress: Tenth International Symposium on Robotics with Applications*, vol. 15, pp. 105–110. <https://doi.org/10.1109/WAC.2004.185205>

11. M. Chalon, M. Grebenstein, T. Wimböck, G. Hirzinger, The thumb: guidelines for a robotic design, in *2010 IEEE/RSJ International Conference on Intelligent Robots and Systems (IROS)*, pp. 2153–2858. <https://doi.org/10.1109/IROS.2010.5650454>
12. M. Chalon, A. Wedler, A. Baumann, W. Bertleff, A. Beyer, J. Butterfaß, M. Grebenstein, R. Gruber, F. Hacker, E. Krämer, K. Landzettel, M. Maier, H.-J. Sedlmayr, N. Seitz, F. Wappeler, B. Willberg, T. Wimböck, G. Hirzinger, F. Didot, Dexhand: a space qualified multi-fingered robotic hand, in *2011 IEEE International Conference on Robotics and Automation*, pp. 2204–2210. <https://doi.org/10.1109/ICRA.2011.5979923>
13. M. Chalon, W. Friedl, J. Reinecke, T. Wimböck, A. Albu-Schaeffer, Impedance control of a non-linearly coupled tendon driven thumb, in *2011 IEEE/RSJ International Conference on Intelligent Robots and Systems (IROS)*, pp. 4215–4221. <https://doi.org/10.1109/IROS.2011.6094542>
14. M. Chalon, A. Dietrich, M. Grebenstein, The thumb of the anthropomorphic Awipi Hand: from concept to evaluation. *Int. J. Robot. Res.* **11**(3), 1450019 (2014). <https://doi.org/10.1142/S0219843614500194>
15. M. Chalon, M. Maier, W. Bertleff, A. Beyer, R. Bayer, W. Friedl, P. Neugebauer, T. Obermeier, H. Sedlmayr, N. Seitz, A. Stemmer, Spacehand: a multi-fingered robotic hand for space, in *ESA Workshop on Advanced Space Technologies for Robotics and Automation – ASTRA*, 2015
16. Z. Chen, N.Y. Lii, T. Wimböck, S. Fan, M. Jin, C. Borst, H. Liu, Experimental study on impedance control for the five-finger dexterous robot hand DLR-HIT II, in *2010 IEEE/RSJ International Conference on Intelligent Robots and Systems (IROS)*, pp. 5867–5874. <https://doi.org/10.1109/IROS.2010.5649356>
17. Z. Chen, T. Wimböck, M.A. Roa, B. Pleintinger, M. Neves, C. Ott, C. Borst, N.Y. Lii, An adaptive compliant multi-finger approach-to-grasp strategy for objects with position uncertainties, in *2015 IEEE International Conference on Robotics and Automation*, pp. 4911–4918. <https://doi.org/10.1109/ICRA.2015.7139881>
18. M.R. Cutkosky, On grasp choice, grasp models, and the design of hands for manufacturing tasks. *IEEE Trans. Robot. Autom.* **5**(3), 269–279 (1989). <https://doi.org/10.1109/70.34763>
19. M.A. Diftler, J.S. Mehling, M.E. Abdallah, N.A. Radford, L.B. Bridgwater, A.M. Sanders, R.S. Askew, D.M. Linn, J.D. Yamokoski, F.A. Permenter, B.K. Hargrave, R. Piatt, R.T. Savely, R.O. Ambrose, Robonaut 2 – the first humanoid robot in space, in *2011 IEEE International Conference on Robotics and Automation (ICRA)*, pp. 2178–2183. <https://doi.org/10.1109/ICRA.2011.5979830>
20. T. Feix, *Human Grasping Database* (2010). <http://grasp.xief.net/documents/taxonomy.pdf> (visited on 30 Sept 2017)
21. T. Feix, H.-B. Schmiedmayer, J. Romero, D. Kragic, A comprehensive grasp taxonomy, in *Robotics: Science and Systems V; Workshop on Understanding Human Hand for Advancing Robotic Manipulation*
22. W. Friedl, M. Chalon, J. Reinecke, M. Grebenstein, FAS a flexible antagonistic spring element for a high performance over actuated hand, in *2011 IEEE/RSJ International Conference on Intelligent Robots and Systems (IROS)*, pp. 1366–1372. <https://doi.org/10.1109/IROS.2011.6094569>
23. W. Friedl, M. Chalon, J. Reinecke, M. Grebenstein, FRCEF: the new friction reduced and coupling enhanced finger for the Awipi hand, in *2015 IEEE-RAS 15th International Conference on Humanoid Robots (Humanoids)*, pp. 140–147. <https://doi.org/10.1109/HUMANOIDS.2015.7363527>
24. H. Gray, *Anatomy of the Human Body*, ed. by Henry Gray, 20th edn., thoroughly rev. and re-edited by Warren H. Lewis (Lea & Febiger, Philadelphia, 1918)
25. H. Gray, *Anatomy, Descriptive and Surgical*, 1901 Edition, ed. by T.P. Pick, R. Howden (Courage Books, Philadelphia, 1999). ISBN:0-76240673-9
26. M. Grebenstein, *Approaching Human Performance: The Functionality – Driven Awipi Robot Hand*. Springer Tracts in Advanced Robotics (Springer, Berlin/Heidelberg/New York, 2014). ISBN:3319035924

27. M. Grebenstein, P. van der Smagt, Antagonism for a highly anthropomorphic hand-arm system, in *Advanced Robotics 22.1: On Robotic Platforms for Research in Neuroscience, Part 2*, 2008, pp. 39–55. ISSN:0169-1864. <https://doi.org/10.1163/156855308X291836>
28. M. Grebenstein, M. Chalon, G. Hirzinger, R. Siegwart, Antagonistically driven finger design for the anthropomorphic DLR Hand Arm System, in *2010 10th IEEE-RAS International Conference on Humanoid Robots (Humanoids)*. <https://doi.org/10.1109/ICHR.2010.5686342>
29. M. Grebenstein, A. Albu-Schäffer, T. Bahls, M. Chalon, O. Eiberger, W. Friedl, R. Gruber, S. Haddadin, U. Hagn, R. Haslinger, H. Höppner, S. Jörg, M. Nickl, A. Nothelfer, F. Petit, J. Reill, N. Seitz, T. Wimböck, S. Wolf, T. Wüsthoff, G. Hirzinger, The DLR Hand Arm System, in *2011 IEEE International Conference on Robotics and Automation (ICRA)*. <https://doi.org/10.1109/ICRA.2011.5980371>
30. M. Grebenstein, M. Chalon, W. Friedl, S. Haddadin, T. Wimböck, G. Hirzinger, R. Siegwart, The hand of the DLR Hand Arm System: designed for interaction. *Int. J. Robot. Res.* **31**(13), 1531–1555 (2012); Towards autonomous physical human-robot interaction. <https://doi.org/10.1177/0278364912459209>
31. S. Haidacher, J. Butterfaß, M. Fischer, M. Grebenstein, K. Jöhl, K. Kunze, M. Nickl, N. Seitz, G. Hirzinger, DLR Hand II: hard – and software architecture for information processing, in *2003 IEEE International Conference on Robotics and Automation (ICRA)*, vol. 1, pp. 684–689. <https://doi.org/10.1109/ROBOT.2003.1241673>
32. K. Hertkorn, B. Weber, P. Kremer, M.A. Roa, C. Borst, Assistance for telepresence using online grasp planning, in *2013 13th IEEE-RAS International Conference on Humanoid Robots (Humanoids)*, pp. 507–513. <https://doi.org/10.1109/HUMANOIDS.2013.7030021>
33. G. Hirzinger, ROTEX—the first space robot technology experiment, in *Experimental Robotics III*. Lecture Notes in Control and Information Science 200 (Springer, New York, 1994), pp. 579–598. ISBN:978-3-540-19905-2
34. G. Hirzinger, B. Brunner, J. Dietrich, J. Heindl, ROTEX—the first remotely controlled robot in space, in *IEEE International Conference on Robotics and Automation*, vol. 3, 1994, pp. 2604–2611. <https://doi.org/10.1109/ROBOT.1994.351121>
35. G. Hirzinger, J. Butterfaß, S. Knoch, H. Liu, DLR’s multisensory articulated hand, in: *Experimental Robotics V, The Fifth International Symposium Barcelona, Catalonia, 15–18 June 1997*, ed. by A. Casals, A.T. de Almeida. Lecture Notes in Control and Information Science 232 (Springer, Berlin, 1998), pp. 47–55. ISBN:3-540-76218-3
36. H. Iwata, S. Sugano, Design of human symbiotic robot TWENDY-ONE, in *2009 IEEE International Conference on Robotics and Automation*, pp. 580–586. <https://doi.org/10.1109/ROBOT.2009.5152702>
37. S.C. Jacobsen, J. Wood, D. Knutti, K. Biggers, UTAH/MIT dexterous hand – work in progress. *Int. J. Robot. Res.* **3**(4), 21–50 (1984). <https://doi.org/10.1177/027836498400300402>
38. S.C. Jacobsen, H. Ko, E. Iversen, C. Davis, Antagonistic control of a tendon driven manipulator, in *1989 IEEE International Conference on Robotics and Automation*, vol. 3, pp. 1334–1339. <https://doi.org/10.1109/ROBOT.1989.100165>
39. I.A. Kapandji, *The Physiology of the Joints: Volume 1 Upper Limb*, 5th edn. vol. 1, With an intro. by F. Poilleux (Edinburgh, Churchill Livingstone, 1982). ISBN:0-443-02504-5
40. A. Kargov, T. Asfour, C. Pylatiuk, R. Oberle, H. Klosek, S. Schulz, K. Regenstein, G. Brethauer, R. Dillmann, Development of an anthropomorphic hand for a mobile assistive robot, in *9th International Conference On Rehabilitation Robotics (ICORR 2005)*, pp. 182–186. <https://doi.org/10.1109/ICORR.2005.1501080>
41. H. Liu, P. Meusel, J. Butterfaß, G. Hirzinger, DLR’s multisensory articulated hand. II: the parallel torque/position control system, in *IEEE International Conference on Robotics and Automation*, 1999, pp. 1904–1909. <https://doi.org/10.1109/ROBOT.1998.680626>
42. H. Liu, K. Wu, P. Meusel, N. Seitz, G. Hirzinger, M. Jin, Y. Liu, S. Fan, T. Lan, Z. Chen, Multisensory five-finger dexterous hand: the DLR/HIT Hand II, in *IEEE/RSJ International Conference on Intelligent Robots and Systems (IROS)*, 2008, pp. 3692–3697. <https://doi.org/10.1109/IROS.2008.4650624>

43. F. Lotti, P. Tiezzi, G. Vassura, L. Biagiotti, C. Melchiorri, UBH 3: an anthropomorphic hand with simplified endo-skeletal structure and soft continuous fingerpads, in: *2004 IEEE International Conference on Robotics and Automation (ICRA)*, vol. 5, pp. 4736–4741. <https://doi.org/10.1109/ROBOT.2004.1302466>
44. F. Lotti, P. Tiezzi, G. Vassura, L. Biagiotti, C. Melchiorri, G. Palli, UBH 3: a biologically inspired robotic hand, in *Intelligent Manipulation and Grasping: International Conference*, ed. by R. Molino, 2004, pp. 39–45
45. F. Lotti, P. Tiezzi, G. Vassura, L. Biagiotti, C. Melchiorri, G. Palli, UBH 3: an anthropomorphic hand with simplified endo-skeletal structure and soft continuous fingerpads, in *2004 IEEE International Conference on Robotics and Automation*, vol. 5, pp. 4736–4741. <https://doi.org/10.1109/ROBOT.2004.1302466>
46. F. Lotti, P. Tiezzi, G. Vassura, L. Biagiotti, G. Palli, C. Melchiorri, Development of UB Hand 3: early results, in: *2005 IEEE International Conference on Robotics and Automation (ICRA)*, pp. 4488–4493. <https://doi.org/10.1109/ROBOT.2005.1570811>
47. C.S. Lovchik, M.A. Diftler, The Robonaut Hand: a dexterous robot hand for space, in *1999 IEEE International Conference on Robotics and Automation*, vol. 2, pp. 907–912. <https://doi.org/10.1109/ROBOT.1999.772420>
48. J. Napier, *Hands*, ed. by J. Russel (Princeton University Press, Princeton, 1993). ISBN:0-691-02547-9
49. O.A. Nierop van, A. van der Helm, K.J. Overbeeke, T.J. Djajadiningrat, A natural human hand model. *The Visual Computer* **24**(1), 31–44 (2008). <https://doi.org/10.1007/s00371-007-0176-x>
50. T. Okada, S. Tsuchiya, On a versatile finger system, in *International Symposium Industrial Robots (JIRA)*, 1977, pp. 345–352
51. Oxford University Press, *Definition for Anthropomorphism – Oxford Dictionaries Online (World English)*. 2012. <http://oxforddictionaries.com/definition/anthropomorphism?q=anthropomorphism> (visited on 30 Sept 2017)
52. Oxford University Press, *Definition for Humanoid – Oxford Dictionaries Online (World English)*. 2012. <http://oxforddictionaries.com/definition/humanoid?q=humanoid> (visited on 30 Sept 2017)
53. H. Ponting, *Ein Fakir in Benares (Varanasi), Indien*. 1907. http://www.geocities.com/blackinkal4/RoyalGeographicalSociety_Asia_2.html (visited on 28 Jul 2017)
54. J. Reinecke, M. Chalon, W. Friedl, M. Grebenstein, Guiding effects and friction modeling for tendon driven systems, in *2014 IEEE International Conference on Robotics and Automation (ICRA)*, pp. 6726–6732. <https://doi.org/10.1109/ICRA.2014.6907852>
55. M.A. Roa, Z. Chen, I. Staal, J. Muirhead, A. Maier, B. Pleintinger, C. Borst, N. Lii, Towards a functional evaluation of manipulation performance in dexterous robotic hand design, in *2014 IEEE International Conference on Robotics and Automation (ICRA)*, pp. 6800–6807. <https://doi.org/10.1109/ICRA.2014.6907863>
56. B. Rubinger, M. Brousseau, J. Lymer, C. Gosselin, T. Laliberte, J.C. Piedboeuf, A novel robotic hand – SARAH for operations on the International Space Station, in: *ESA Workshop on Advanced Space Technologies for Robotics and Automation*, 2002
57. K.J. Salisbury, B. Roth, Kinematics and force analysis of articulated mechanical hands, Ph.D. Thesis, Stanford, Stanford University, 1982
58. S. Schulz, C. Pylatiuk, G. Brethauer, A new ultralight anthropomorphic hand, in *2001 IEEE International Conference on Robotics and Automation (ICRA)*, vol. 3, pp. 2437–2441. <https://doi.org/10.1109/ROBOT.2001.932988>
59. T. Sugaiwa, H. Iwata, S. Sugano, A motion control for dexterous manipulation with human mimetic hand-arm system, in *9th IEEE-RAS International Conference on Humanoid Robots (Humanoids, 2009)*, pp. 653–659. <https://doi.org/10.1109/ICHR.2009.5379511>
60. T. Wimböck, C. Ott, G. Hirzinger, Passivity-based object-level impedance control for a multifingered hand, in *IEEE International Conference on Intelligent Robots and Systems (IROS)*, 2006, pp. 4621–4627. <https://doi.org/10.1109/IROS.2006.282170>

-
61. T. Wimböck, C. Ott, A. Albu-Schäffer, G. Hirzinger, Comparison of object level grasp controllers for dynamic dexterous manipulation. *Int. J. Robot. Res.* **31**(1), 3–23 (2012). <https://doi.org/10.1177/0278364911416526>
 62. S. Wolf, G. Hirzinger, A new variable stiffness design: matching requirements of the next robot generation, in *2008 IEEE International Conference on Robotics and Automation (ICRA)*, pp. 1741–1746. <https://doi.org/10.1109/ROBOT.2008.4543452>
 63. S. Wolf, O. Eiberger, G. Hirzinger, The DLR FSJ: energy based design of a variable stiffness joint, in *2011 IEEE International Conference on Robotics and Automation (ICRA)*, pp. 5082–5089. <https://doi.org/10.1109/ICRA.2011.5980303>



Underactuation with Link Mechanisms

Clément Gosselin

Contents

1	Introduction	524
2	Kinematic and Static Modeling	526
3	Example Designs	527
3.1	Two-Phalanx Five-Bar Underactuated Finger	527
3.2	Three-Phalanx 3-dof Underactuated Finger	528
3.3	Three-Fingered Underactuated Hands	529
4	Future Directions	533
	References	533

Abstract

This section discusses the use of mechanical linkages in the design of underactuated robotic hands. First, a literature review is provided that introduces the main contributions in this area. Then, a static analysis is briefly described, and a model that can be used for analysis and synthesis of linkage-based underactuated fingers is developed. Two examples of underactuated fingers with, respectively, two and three phalanges are then introduced in order to demonstrate the application of the model and to raise the main design issues. Examples of underactuated hands based on these underactuated fingers are then described, and some existing prototypes are presented.

C. Gosselin (✉)

Department of Mechanical Engineering, Université Laval, Québec, QC, Canada
e-mail: gosselin@gmc.ulaval.ca

1 Introduction

The development of versatile robotic hands that are capable of grasping a wide variety of objects using simple high-level commands is of great interest in humanoid robotics. Such hands can be obtained with the help of underactuation. An underactuated mechanism is one which has fewer actuators than degrees of freedom (dofs). When applied to mechanical fingers, the concept of underactuation leads to self-adaptability. Self-adaptive fingers have the capability to envelope the objects to be grasped and automatically adapt to their shape with few actuators and without complex control strategies. In order to obtain a statically determinate system, elastic components and mechanical limits are introduced in underactuated mechanisms. While a finger is closing on an object, the configuration of the finger at any time is determined by the external constraints associated with the object. When the object is fully grasped, the force applied at the actuator is distributed among the phalanges. It is pointed out that the elastic components generally have a negligible impact on the grasping itself. Their purpose is mainly to return the fingers to a determinate open configuration when there is no contact with an object.

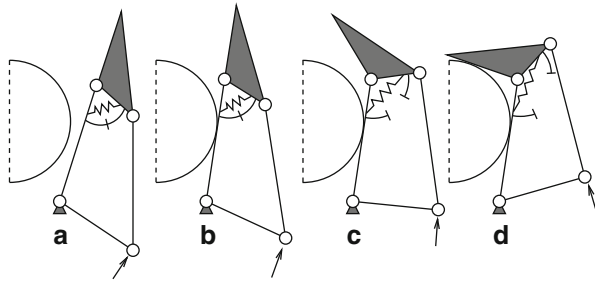
A large number of underactuated fingers and hands have been proposed in the literature (see [5] for an exhaustive literature review). Many of the proposed underactuated fingers are based on tendon transmissions or compliant mechanisms. Although tendon-driven and compliant hands can lead to effective and compact designs, they are generally limited to relatively small grasping forces. Also, tendon systems are prone to friction and elasticity, which limit their performance. As humanoid robotics is moving toward more powerful designs (approaching human force capabilities), it is desirable to target hands with significant force capabilities.

In order to alleviate the drawbacks of tendon transmissions, the use of linkage-based underactuated fingers was also proposed in the literature. In [16], the authors proposed a system composed of two fingers, each having 2 dofs, and provided a detailed static analysis that demonstrated the advantages of linkage-based underactuated hands. In [3], an underactuated hand with three fingers was presented. Each of the fingers is based on a 2-dof mechanism having two phalanges and one actuator. Additionally, a special mechanism is introduced in order to allow the distal phalanges to be maintained orthogonal to the palm when precision grasps are performed. In [6], a linkage-based underactuated hand resembling the human hand was presented. Each of the fingers is composed of three phalanges but has only 2 dofs since the motion of the last phalanx is directly coupled to the motion of the second phalanx. In [9], an underactuated planar mechanical hand with two fingers was proposed that is capable of mechanically avoiding obstacles before grasping an object. The static analysis and the design of underactuated fingers and hands based on a 2-dof underactuated linkage were developed in [12]. The results were extended to 3-dof underactuated fingers in [13] and [4,5,11]. Several underactuated hands were built based on these references, namely, the MARS hand [7] which has 12 dofs and 6 actuators and was developed for industrial applications, the

SARAH hand [14] which has 10 dofs and 2 actuators and was developed for space applications, and the UKAEA hand [8] which also has 10 dofs and 2 actuators and was developed for the nuclear industry. All of these prototypes were developed for large payloads and grasping forces (for instance, the UKAEA hand has a payload capacity of 100 kg), which required the use of linkage-based fingers. Indeed, such force capabilities cannot be envisioned with tendon-based mechanisms. A version of the SARAH hand was commercialized by Robotiq [1] and it is used in many industrial applications. This hand is appropriate for humanoid robotics applications, especially when large forces and robustness are required. As an example, several of the teams participating to the 2015 DARPA Robotics Challenge [2] used the Robotiq hand on their prototypes.

This section presents the basic analysis tools that are required to model linkage-based underactuated fingers. It also provides design examples that clearly illustrate how such mechanisms can be effectively used to build underactuated hands. The general principle of a linkage-based underactuated finger is illustrated in Fig. 1, where a simple two-phalanx five-bar underactuated finger is represented. At rest, the two phalanges are maintained in an aligned configuration by an extension spring and a mechanical limit (in *a*). The actuator, represented by the arrow on the figure, is then used to close the finger on an object. When contact is established between the object and the first phalanx (in *b*), the actuator force then extends the spring, which separates the mechanical limit (in *c*), and contact is then established between the object and the distal phalanx (in *d*). The actuator force is then distributed between the two phalanges, and the finger has adapted to the shape of the object, by mere mechanical conformation. This adaptation is sometimes referred to as mechanical intelligence. It should be pointed out that when the shape adaptation phase is completed, the elastic components included in the finger play a negligible role in the force distribution. Indeed, the elastic components are used to determine the motion of the fingers when no contacts are established with objects. Typically, the elastic components are used to maintain the fingers open, with the free links resting on mechanical limits. Therefore, they are often neglected in static analyses, which is a reasonable assumption. Another characteristic of linkage-based underactuated fingers is apparent from Fig. 1. Indeed, it can be observed that when the configuration of such a finger changes, its transmission properties (Jacobian matrix) also change. In other words, the transmission ratios between the actuator and the contact forces at the phalanges change. This is due to the use of linkages. By contrast, in tendon-driven systems, the transmission ratios are usually constant and are adjusted by selecting the diameters of the transmission pulleys. This characteristic makes the design of linkage-based fingers more challenging. Finally, it can also be observed, from Fig. 1, that designing compact linkage-based fingers is a challenge since linkages tend to require more space than pulleys and tendons. Despite these challenges, the advantages of linkage-based fingers mentioned above (large force capability, low friction) are largely worth the effort and the examples provided in this section clearly demonstrate that very effective linkage-based underactuated hands can be designed based on the presented approach.

Fig. 1 Grasping sequence of a two-phalanx underactuated finger based on a five-bar linkage



2 Kinematic and Static Modeling

A reasonable assumption applying to the vast majority of robotic hands is that their motion is slow enough to make their dynamics negligible. Indeed, the inertial forces induced by the motion of the phalanges of a hand are generally very small compared to the grasping forces. Therefore, the dynamics of the system are not considered, and a static model is sufficient to characterize the behavior of the hand grasping an object. Following this assumption, the derivation of a general static model of an underactuated finger – which is readily generalized to an underactuated hand – is now outlined. The reason for including kinematic quantities, namely, velocities, instead of only static variables is the use of the principle of virtual work, which allows a convenient and elegant elimination of the constraint forces acting on the links.

Let \mathbf{t} be the vector of actuator and elastic torques at the joints and $\dot{\boldsymbol{\theta}}$ be the corresponding vector of actuated joint velocities. Also, let vector \mathbf{f} be the vector of external forces (normally grasping forces) while vector $\dot{\mathbf{c}}$ is the vector containing the corresponding velocity components, each component being defined along the corresponding external force. The input and output virtual powers can then be equated, yielding

$$\mathbf{t}^T \dot{\boldsymbol{\theta}} = \mathbf{f}^T \dot{\mathbf{c}}. \quad (1)$$

Since elastic components are used to determine the configuration of the finger in the absence of contacts, the number of such components, combined with the number of actuators, must be sufficient to lead to a statically determined system. Hence, one has

$$\dot{\mathbf{c}} = \mathbf{J}\dot{\boldsymbol{\gamma}} \quad (2)$$

where $\boldsymbol{\gamma}$ is a vector of selected coordinates that is used to fully describe the configuration of the finger and where \mathbf{J} is a square matrix that is invertible in general configurations. Vector $\boldsymbol{\gamma}$ is usually chosen to be the vector of joint coordinates corresponding to the motion of the phalanges. Moreover, vector $\dot{\boldsymbol{\gamma}}$ can be related to vector $\dot{\boldsymbol{\theta}}$ through another Jacobian matrix, namely,

$$\dot{\gamma} = \mathbf{K}\dot{\theta} \quad (3)$$

where \mathbf{K} is a square matrix that is invertible in general configurations. Substituting Eqs. (2) and (3) into Eq. (1), one then obtains

$$\mathbf{t}^T \dot{\theta} = \mathbf{f}^T \mathbf{J} \mathbf{K} \dot{\theta}. \quad (4)$$

According to the principle of virtual work, since Eq. (4) must be valid for any vector $\dot{\theta}$, one then finally obtains

$$\mathbf{t} = \mathbf{K}^T \mathbf{J}^T \mathbf{f}. \quad (5)$$

Equation (5) provides the relationship between the actuator (and elastic) torques and the contact forces. Since matrices \mathbf{J} and \mathbf{K} are both square and generally invertible, the above relationship can also be inverted, which is useful for simulation and design.

3 Example Designs

3.1 Two-Phalanx Five-Bar Underactuated Finger

One of the simplest designs of a linkage-based underactuated finger is obtained by considering the five-bar linkage shown in Fig. 2. This architecture was studied extensively in [12] and later in [5, 11]. Following the notation used in Fig. 2 and neglecting the elastic forces, the contact forces F_k and F_j at the phalanges can be obtained using the derivation presented in the preceding section, yielding

$$F_k = \frac{(j_c - h \cos \theta)k}{ak_c j_c (\cot \beta \cos \eta + \sin \eta)} T_a, \quad (6)$$

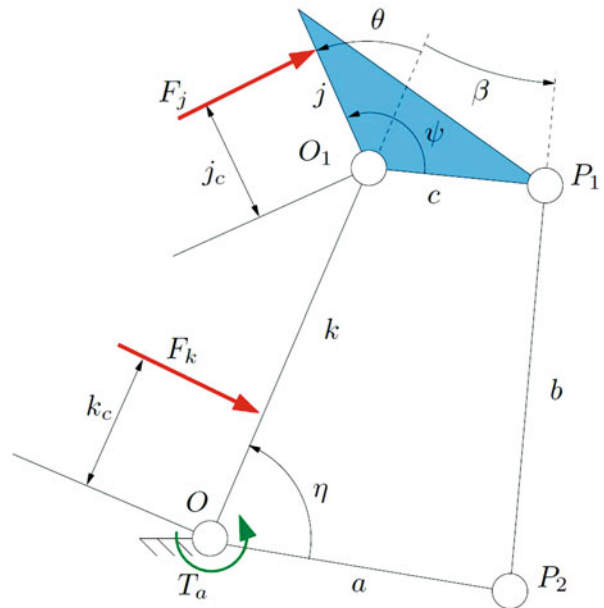
$$F_j = \frac{h}{aj_c (\cot \beta \cos \eta + \sin \eta)} T_a \quad (7)$$

where $h = c(\cos(\theta - \psi) - \sin(\theta - \psi) \cot \beta)$ is the distance between point O_1 and the intersection of lines (OO_1) and $(P_1 P_2)$. Also, η is the angle between link a and the first phalanx. Such expressions can be used to study the conditions under which both F_k and F_j are positive, corresponding to enveloping grasps. The geometric parameters of the fingers can then be adjusted in order to produce the desired behavior.

In some situations, the contact with the first phalanx may be lost. However, there exists a position of the contact point on the distal phalanx, noted j_c , for which this situation still corresponds to a stable grasp. Indeed, the distal phalanx is then subjected to three pure forces; thus, equilibrium can only exist if they all intersect in a common point. Static analysis shows that this contact position is given as

$$j_c = e = c \cos \theta (\cos(\theta - \psi) - \sin(\theta - \psi) \cot \beta) \quad (8)$$

Fig. 2 Geometric modeling of a two-phalanx underactuated finger based on a five-bar linkage



with the corresponding contact force being

$$F_j = \frac{T_a}{a \cos \theta (\sin \eta + \cos \eta \cot \beta)}. \quad (9)$$

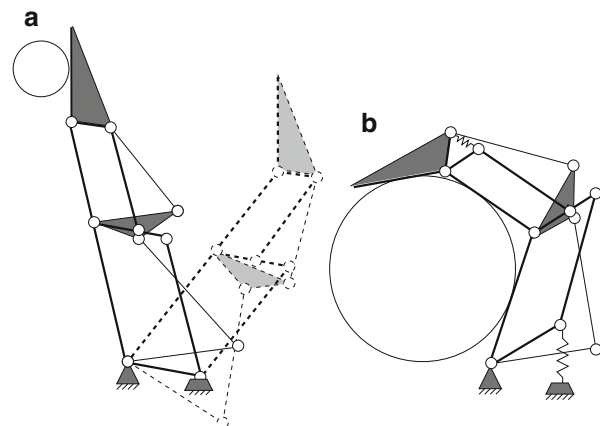
Physically, the above expression implies that the contact force should be located on the projection onto the distal phalanx of the intersection of lines (OO_1) and (P_1P_2). Based on the above expressions, grasping sequences can also be studied, and stability diagrams can be obtained (see, for instance, [5, 11]) that represent the feasibility of one-contact grasps (or pinch grasps) and the ability of a finger to converge to such stable grasps.

It is pointed out that the geometry of the linkages is crucial in obtaining a desired behavior. Indeed, if the geometric parameters are not properly chosen, the objects may be ejected instead of being properly grasped. As discussed in [5, 12], it is possible to optimize the parameters to prevent the ejection phenomenon. This phenomenon was pointed out in [12, 15] and is related to the self-posture changeability of mechanisms described in [10].

3.2 Three-Phalanx 3-dof Underactuated Finger

The concept of linkage-based underactuated finger presented above was extended to three-phalanx fingers in [7], as illustrated in Fig. 3. Expressions – similar to those given above for the two-phalanx finger – for the forces at the different phalanges can be obtained using the static model. These expressions can be used to select the

Fig. 3 A three-phalanx linkage-based underactuated finger including a parallel mechanism for pinch grasps



design parameters of the finger. In [11–13], the design of a three-phalanx finger was studied in detail. It was shown that some of the link ratios are crucial to obtaining a proper behavior of the finger. Optimization indices were defined based on these observations, and optimum designs were presented.

An additional linkage consisting in a series of parallelograms is introduced in the finger represented in Fig. 3. This mechanism aims at providing the capability for underactuated fingers to perform precision grasps (pinch grasps) while maintaining the distal phalanges parallel to each other, for objects of different sizes. This feature allows more stable grasps when only the tips of the fingers are used and is very often feasible with simple grippers. A mechanism has been proposed in order to achieve this behavior for a 2-dof underactuated finger in [3]. A mechanism achieving a similar behavior with the third phalanx of a 3-dof underactuated finger has been developed in [7] and is illustrated in Fig. 3. It is composed of two parallelograms mounted in series. This mechanism is coupled to the phalanges of the finger but not to the other links of the shape adaptation mechanism (it is moving on a parallel plane). Two mechanical limits with springs at the top and bottom ends of the mechanism allow precision grasps to be performed and the adaptation to power grasps if necessary. This is illustrated in Fig. 3. In configurations (a), from dashed lines to full lines, a parallel motion of the distal phalanx is accomplished, by maintaining the parallelogram mechanism on its mechanical limits. In (b), a power grasp is performed, with contacts on all phalanges. In this case, the parallelogram mechanism is moved away from its mechanical limits and the distal phalanx is no longer maintained parallel.

3.3 Three-Fingered Underactuated Hands

The three-phalanx finger described in the preceding subsection was used in the design of several linkage-based underactuated hands. Three such fingers are mounted on a common base which is used as a palm. Each of the three identical

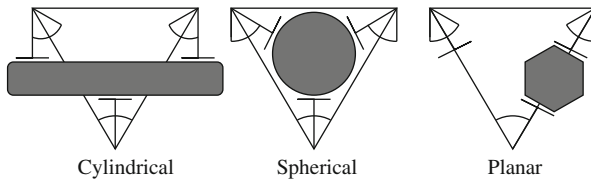
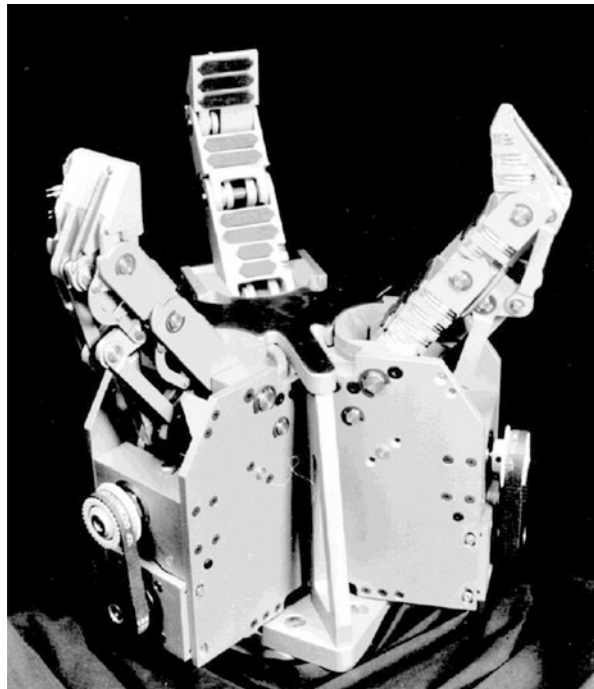


Fig. 4 Main configurations of fingers (top view)

Fig. 5 Photograph of the 12-dof 6-doa Mars hand



fingers is mounted on an additional revolute joint whose axis is located on the vertex of an equilateral triangle and oriented normal to the plane of the triangle. With these additional revolute joints, the hands can be reconfigured by modifying the orientation of the fingers in order to adapt to the general geometry of the object to be grasped. This feature is in fact widely used in the literature. The main grasping configurations of the fingers are: cylindrical, spherical and planar. In the cylindrical configuration, two fingers point in the same direction while the third one points in the opposite direction and moves between the other two. In the spherical configuration, the three fingers are oriented toward the center of the triangle. In the planar configuration, two fingers are directly facing each other and the third finger is not used. The main grasping configurations are represented schematically in Fig. 4.

The first underactuated hand to be built using the above described arrangement is the MARS hand, shown in Fig. 5. This hand has 12 dofs and 6 degrees of actuation

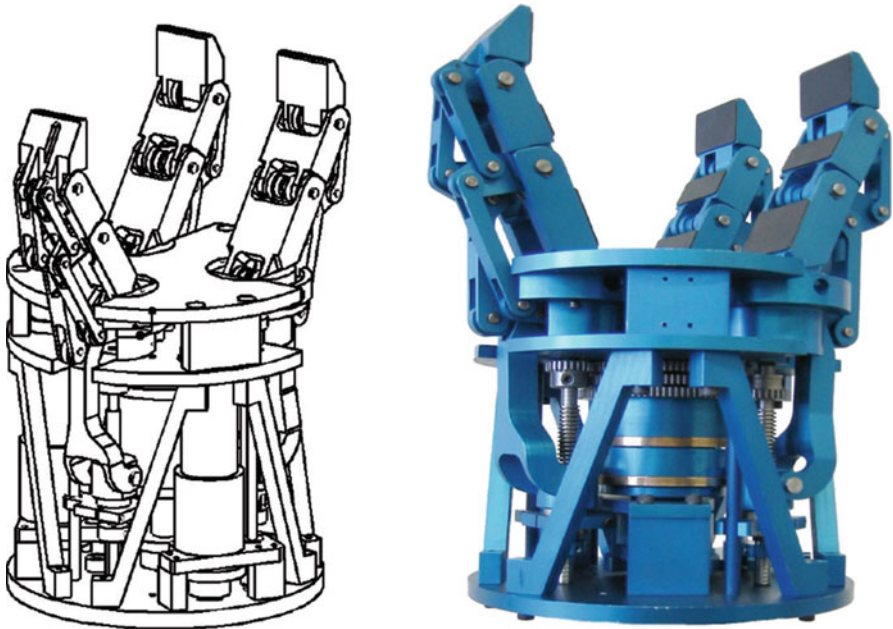


Fig. 6 CAD model and photograph of the 10-dof 2-doa SARAH hand

(doas). Each finger includes one actuator for the closing motion and one actuator for the rotation of the finger around the base. Therefore, in addition to the main grasping configurations shown in Fig. 4, several other relative orientations of the fingers are feasible. Indeed, the three fingers can be freely rotated within a range of 60 degrees, as illustrated in Fig. 4. This rotation is performed by a small gearmotor coupled to a gear attached to the base. The transmission of the motor to the finger (for the closing motion) is composed of a ballscrew in order to obtain large forces and a timing belt in order to obtain compact modules and allow the modification of the transmission ratio. Note that since a ballscrew is used, the fingers are backdrivable. This is useful in applications where the grasping force must be controlled.

Driven by the contingencies of space applications and in order to further improve the compactness as well as reducing the control complexity, hands including fewer actuators were then designed, based on the three-phalanx underactuated finger described above. The SARAH hand, shown in Fig. 6, and the UKAEA hand each possesses 10 dofs but only 2 doas, which is a considerable reduction. Two main design changes have made this reduction possible. First, by allowing only the most useful finger orientations with respect to the base (Fig. 4), the coupling of the orientation of the fingers is possible. In other words, one gearmotor and a linkage are used to commonly drive the rotation of all fingers. The linkage is designed such that the configurations shown in Fig. 4 are possible. The second design change is the most important: it consists in introducing underactuation between the fingers.

In other words, a single actuator is used to drive the closing motion of all fingers while allowing underactuation between them. The SARAH hand was the first hand to introduce at the same time underactuation within the fingers and between the fingers. In the SARAH hand and the UKAEA hand, the underactuation between the fingers is produced by a one-input/three-output differential, adding two degrees of underactuation. Therefore, if one or two of the fingers are blocked, the remaining fingers continue to close until they properly grasp the object. The force is fully applied only when all the fingers have properly made contact with the object or the palm. The differential mechanism is described in detail in [7].

Finally, it should be mentioned that a modified version of the SARAH hand is commercialized by Robotiq [1] for industrial applications. The Robotiq hand (S model) is shown in Fig. 7.

Fig. 7 Robotiq S-hand
(Photo courtesy of Robotiq)



4 Future Directions

This section demonstrated the advantages and challenges of linkage-based underactuated robotic hands. Several hands based on this principle have been proposed in the literature, including functional prototypes and commercially available products. In the context of humanoid robotics, linkage-based underactuated robotic hands constitute a promising avenue, especially if force capabilities similar or superior to that of human beings are considered. Future research directions include the development of compact mechanisms, as well as the experimentation with different types of joints – including rolling joints – and advanced lightweight and smart materials.

References

1. <http://www.robotiq.com>
2. <http://www.theroboticschallenge.org>
3. S.J. Bartholet, *Reconfigurable End Effector*. US Patent No. 5 108 140 (1992)
4. L. Birglen, C.M. Gosselin, Geometric design of three-phalanx underactuated fingers. ASME J. Mech. Des. **128**(2), 356–364 (2006)
5. L. Birglen, T. Laliberté, C. Gosselin, *Underactuated Robotic Hands*. Springer Tracts in Advanced Robotics (Springer, Berlin, 2008)
6. R.M. Crowder, An anthropomorphic robotic end effector. Robot. Auton. Syst. **7**(4), 253–268 (1991)
7. C. Gosselin, T. Laliberté, *Underactuated Mechanical Finger with Return Actuation*. US Patent No. 5 762 390 (1996)
8. C. Gosselin, T. Laliberté, Underactuated versatile gripper for the cleaning of nuclear sites, in *Proceedings of the 1st International Conference on Applied Robotics for the Power Industry (CARPI)*, Montreal, Oct 2010
9. H. Itoh, *Mechanical Hand*. US Patent No. 3 927 424 (1975)
10. M. Kaneko, T. Hayashi, Standing-up characteristic of contact force during self-posture changing motions, in *Proceedings of the IEEE International Conference on Robotics and Automation*, 1993, pp. 202–208
11. T. Laliberté, L. Birglen, C. Gosselin, Underactuation in robotic grasping hands. Jpn. J. Mach. Intell. Robot. Control Spec. Issue on Underactuated Robot. **4**(3), 77–87 (2002)
12. T. Laliberté, C. Gosselin, Simulation and design of underactuated mechanical hands. Mech. Mach. Theory **33**(1/2), 39–57 (1998)
13. T. Laliberté, C. Gosselin, Development of a three-dof underactuated finger, in *Proceedings of the 2001 CCToMM Symposium on Mechanisms, Machines, and Mechatronics*, Saint-Hubert, June 2001. Available online at http://www.me.uvic.ca/~ram/2001_CCToMM_Symposium/,
14. T. Laliberté, C. Gosselin, *Actuation System for Highly Underactuated Gripping Mechanism*. US Patent No. 6 505 870 (2003)
15. S. Montambault, C. Gosselin, Analysis of underactuated mechanical grippers. ASME J. Mech. Des. **123**(3), 367–374 (2001)
16. H. Shimojima, K. Yamamoto, K. Kawakita, A study of grippers with multiple degrees of mobility. JSME Int. J. **30**(261), 515–522 (1987)